4. Environmental reconstruction of the Middle Pleistocene archaeological/palaeontological site Mata Menge, Flores, Indonesia

G.D. van den Bergh[1], I. Kurniawan[2], M. J. Morwood[1,3], C.J. Lentfer[4], Suyono[2], R. Setiawan[2] & F. Aziz[2]

[1]*School of Earth and Environmental Sciences, University of Wollongong, Wollongong, NSW, Australia 2522*
[2]*Geological Survey Institute, Bandung 40122, Indonesia*
[3]*School of Humanities, University of New England, Armidale, NSW, Australia 2350*
[4]*School of Social Science, University of Queensland, Australia*

Corresponding author: Gert van den Bergh (gert@uow.edu.au)

Keywords: Indonesia, Flores, Pleistocene, sedimentology, palaeontology, archaeology, taphonomy, environmental reconstruction

Abstract

This paper describes the sedimentology and taphonomy of early Middle Pleistocene palaeontological and archaeological deposits at Mata Menge in the Soa Basin of central Flores. The lateral and vertical development of the bone and artefact-bearing sandstone layer, as well as the internal sedimentary structures and fossil content, indicate a lakeshore setting close to a tributary stream. Furthermore, the shoreline at the site was oriented north-south, with clastic influxes (streams, sheet flows, debris flows) entering the lake from the west, and occasionally the lake-margin was also blanketed by volcanic tuff deposited from suspension. Water levels in the lake fluctuated and wave action reshaped the coastal sediments into north-south oriented beach ridges, where bacterial mats grew at the sediment/water interface.

The *Stegodon florensis* bones at Mata Menge mainly resulted from the natural deaths of aged animals on the lakeshore or in the shallows. They were then subject to limited water transport, leading to an over-representation of the less transportable, heavier elements. Exposure and fluvial transport was responsible for some of the damage to the bones prior to burial, but trampling by *Stegodon* visiting the lakeshore probably contributed. Despite the abundance of stone artefacts in the same layers as the *Stegodon* bones, there is no evidence for butchering of the animals by hominins.

4.1. Introduction

From 1957 until the early 1970s, Theodor Verhoeven, a Dutch priest, carried out excavations at a number of palaeontological and archaeological sites in the Soa Basin of central Flores (Maringer and Verhoeven, 1970; Verhoeven, 1968). These included Mata Menge, where he recovered stone artefacts associated with the fossilised remains of rat and *Stegodon* that Hooijer (1957, 1967, 1972)

interpreted as a subspecies of the Javanese *Stegodon* (i.e. *S. trigonocephalus florensis*).

Mata Menge was relocated by an Indonesian-Dutch team, who carried out excavations there in 1992 and 1994 (Sondaar *et al*., 1994). They recovered the remains of *Stegodon*, rat and crocodile, as well as stone artefacts (Sondaar *et al*., 1994; van den Bergh *et al*., 1996). With more detailed analysis, the *Stegodon* from Mata Menge and other Soa Basin sites proved to be a distinct species, *Stegodon florensis*, which is probably most closely related to a large-bodied *Stegodon* from Sulawesi and Sangihe, two islands north of Flores (van den Bergh, 1999).

In 1997, an Indonesian-Australian team collected two tuff samples from Mata Menge, for zircon fission-track dating. The tuffaceous mudstone containing the lowermost vertebrate fossils and stone artefacts at the site yielded an age of 0.88 ± 0.07 Myr BP, while the overlying white tuff yielded an age of 0.80 ± 0.07 Myr BP (Morwood *et al*., 1998). The former now provides a minimum age for hominins on Flores.

More recently, fossil *Stegodon* and hominin remains dating to between 95 and 17 kyr were discovered at Liang Bua, a limestone cave about 40 km west of Mata Menge (Morwood *et al.*, 2004, 2008). The *Stegodon* at Liang Bua appears to be derived from *S. florensis*, and is therefore considered a chrono-subspecies, *Stegodon florensis insularis*, which on average was 30% smaller than its Soa Basin ancestor (van den Bergh *et al*., 2008). The phylogenetic history of the associated hominin, *H. floresiensis*, remains unclear, however. This endemic species was only ~100 cm high with many primitive traits, including a very small brain (400 cc), pronounced supraorbital tori, no chin, ape-like carpal bones and Australopithecine-like body proportions (Brown *et al* 2004; Morwood *et al.*, 2005). The species may have evolved on Flores by insular dwarfing of a *Homo erectus* population, but is more likely to have descended from an earlier hominin species akin to *Homo habilis* (Argue *et al.*, 2007; Brown *et al*., 2004, Falk *et al*., 2005, 2007, Tocheri *et al.*, 2007).

In 2004, 2005 and 2006, further excavations were carried out at Mata Menge (Figs. 4.1a, b and 4.2). The aims were to: 1) Recover skeletal remains of the hominins, who made the stone artefacts and may have been ancestral to *H. floresiensis;* 2) Obtain a larger assemblage of *in situ* stone artefacts; 3) Obtain a larger sample of faunal remains for taphonomic and palaeontological studies; 4) Reconstruct the depositional environment of the fossil and artefact-bearing layers.

Unfortunately, we did not find hominin skeletal remains, but the work significantly increased the number of stone artefacts and faunal remains excavated from Mata Menge, and provided valuable stratigraphic evidence for site formation processes and environmental context. The stone artefacts have been described elsewhere (Brumm *et al.*, 2006; chapter 7, this volume; Moore and Brumm, 2007). This paper concerns the Mata Menge stratigraphy, sedimentology, faunal remains, and their palaeo-environmental implications.

4.2. Local stratigraphy near Mata Menge

Mata Menge is located in the northwestern part of the Soa Basin (Fig. 4.2), where the complete regional stratigraphic sequence is evident, albeit considerably thinner than in the central part of the basin (Fig. 4.3; O'Sullivan *et al.*, 2001). In descending order strata include:

Fig. 4.1. A: General view towards the west of the Mata Menge excavation in 2005. B: The Mata Menge excavation at the end of the 2005 campaign. View is towards the northeast (photo Adam Brumm).

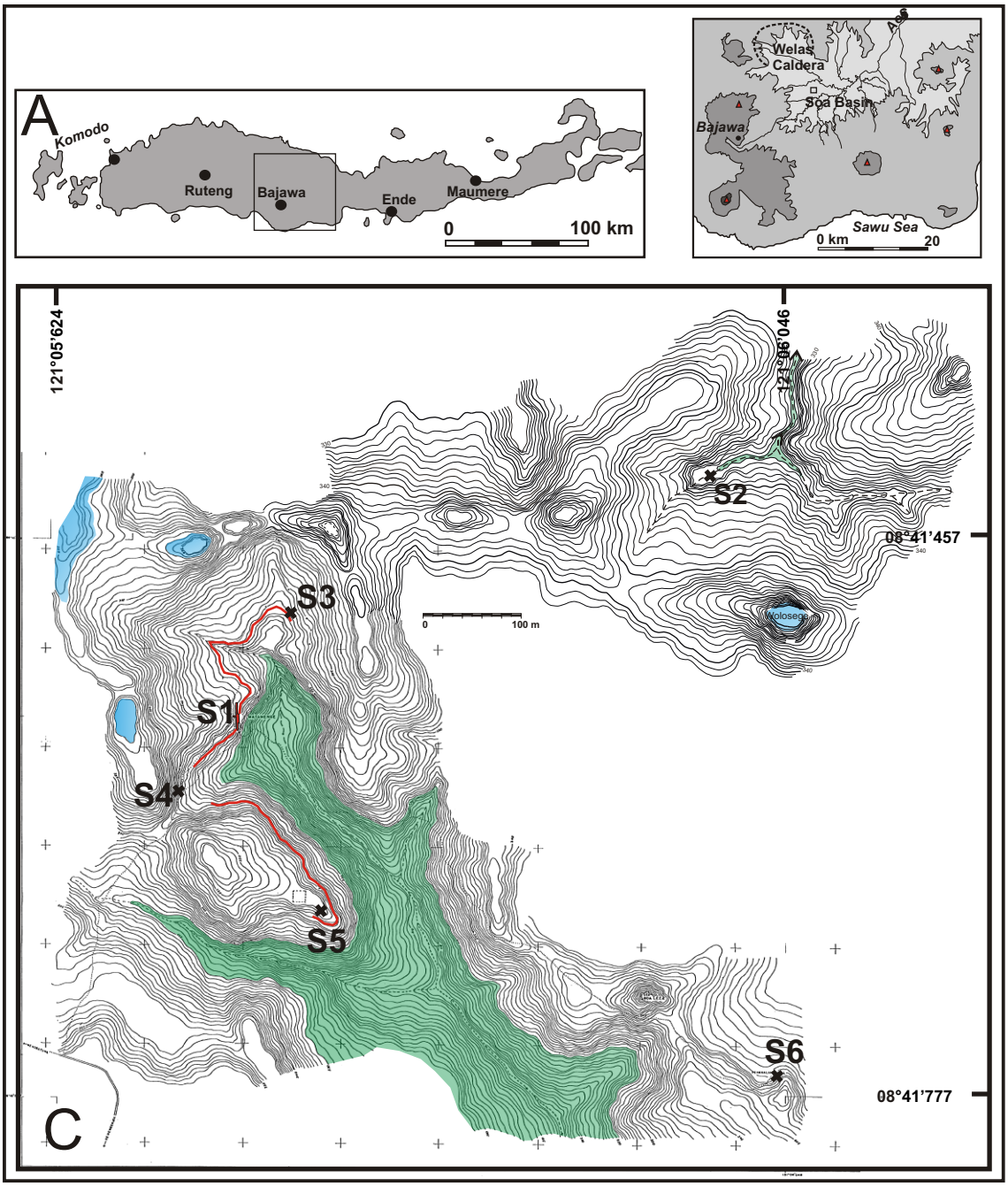

Fig. 4.2. A: Map of Flores with insert indicating the Soa Basin. B: map of the Soa Basin with insert indicating the location of the map shown in C. C: topographic map showing the locations of the Mata Menge (S1), Wolo Sege (S2) and Boaleza (S6) excavations. S3, S4 and S5 indicate the locations of other features mentioned in the text. Red line indicates the extent of the fossil and artefact-bearing layer near Mata Menge. Green is the Ola Kile Fm. Blue is the limestone member of the Ola Bula Fm.

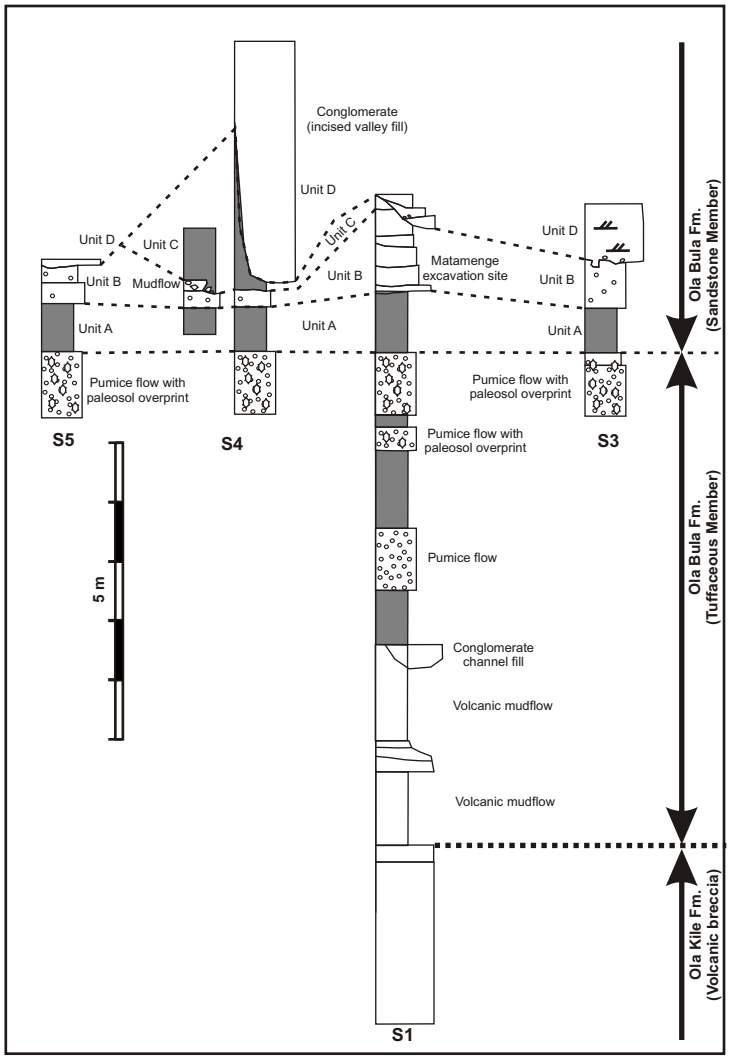

Fig. 4.3. Stratigraphic sections near the Mata Menge excavation site. S1, S3, S4 and S5 refer to the locations indicated in Fig. 4.1. The subdivision of Units A-D is discussed in the text.

a) Thin-bedded micritic lacustrine limestones and multi-coloured marls that cap the Ola Bula Formation (Fm). These are exposed in the hill slope 23 metres above the excavation area. On the east side of the Soa Basin, these limestones yielded fission track ages of 0.68 ± 0.07 and 0.65 ± 0.06 Myr BP (O'Sullivan *et al.*, 2001).

b) Fluvio-lacustrine sandstone and siltstone layers of the middle sandstone member of the Ola Bula Fm. Fossilised faunal remains and stone artefacts occur in the lowest of these layers. A prominent white, tuffaceous silt exposed in the hill slope 18 metres above the excavation area yielded a fission track age of 0.75 ± 0.07 Myr BP, whereas the excavated fossil deposits are 0.88 to 0.80 Myr old (Morwood *et al.*, 1998).

c) White pumice layers of the basal tuff member of the Ola Bula Fm, which alternate with layers of fluvio-lacustrine silty clay and a single 50 cm thick gravel lens. The two uppermost pumice layers are overprinted by red-brown paleosoil. The lowermost yielded a fission track age of 0.94 ± 0.06 Myr BP (O'Sullivan *et al.*, 2001). The basal tuff member of the Ola Bula Fm presumably correlates with the Welas Tuff of Muraoka *et al.* (2002), which they relate to the caldera forming phase of the Welas Caldera located directly northwest of the Soa Basin (see chapter 2).

d) The basement breccias of the Ola Kile Formation, which outcrops 20 m to the south and 10 metres below the excavation area. Nearby, the uppermost part of the Ola Kile Formation yielded a fission track age of 1.86± 0.12 Myr BP (O'Sullivan *et al.*, 2001).

4.3. Methods

During the three successive excavations at Mata Menge (2004-2006), a total of 65.5 square metres of deposit was excavated down to the basal, pink silty clay (Unit A), at a maximum depth of 3.5 m. (Figs. 4.4 and 4.5). A contoured topographic map of the site and surrounds was also prepared with a theodolite and GPS, the fossil-bearing layer was traced laterally and plotted on this map, and the planned excavation area was gridded into quadrants.

After removal of the topsoil, the sandstone and tuffs were excavated using picks, geological hammers and small chisels, as appropriate. Sieving proved impractical, so blocks of stone were broken up and closely examined before being discarded. Stratigraphic drawings were made of the excavation baulks in all sectors, and three-dimensional coordinates were recorded for all larger fossil remains and stone artefacts using a fixed datum and the corners of quadrants as reference

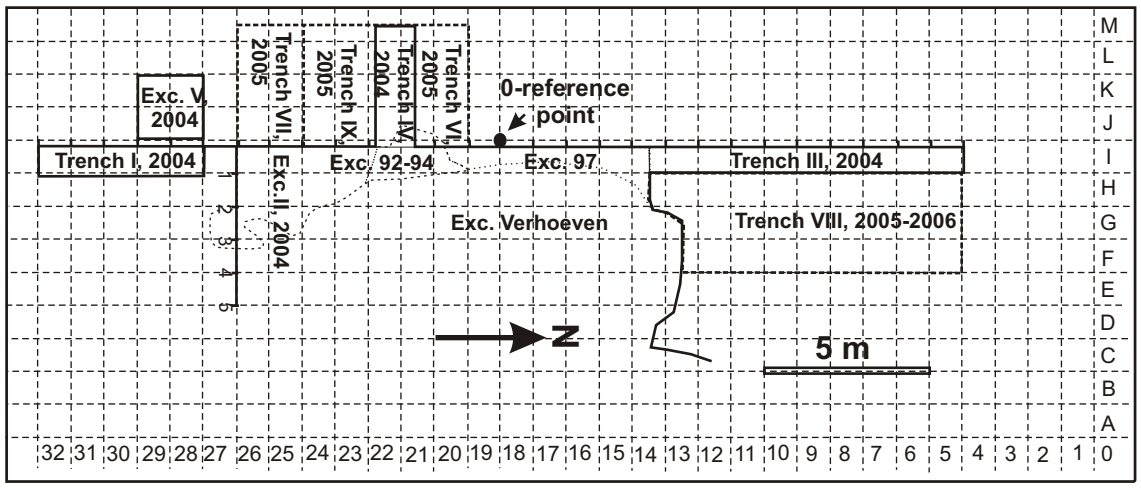

Fig. 4.4. Mata Menge excavation plan, showing the trenches excavated with their year of excavation. Trenches VII and VIII were started in 2005 but were excavated down to the base of the artefact and bone bearing layer in 2006. x and y coordinates of fossils and artefacts were measured relative to the 0 reference point.

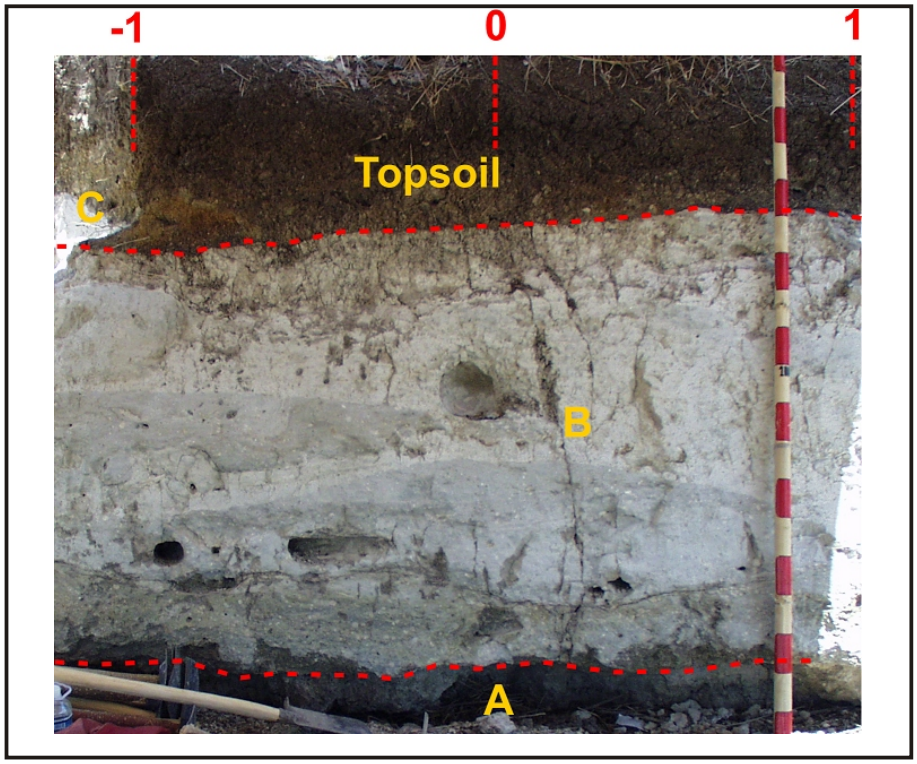

Fig. 4.5. Part of the West baulk of sector II (see also line drawing Fig. 4.9), showing Units A-C. Scale pole is marked with 10-cm intervals. The amalgamated Unit B is fining-upward and has coarse-grained poorly sorted sandstone at the base. These are overlaid by an alternation of sandy lenses and white tuffaceous silts. Cylindrical holes visible in the profile represent empty casts of decayed wood fragments.

points. This allowed the position of fossils and artefacts to be back plotted on the stratigraphic sections as the excavation proceeded.

4.4. Sedimentology of Mata Menge

In the Mata Menge excavation area there is a general sequence of four lithological units, which can be easily distinguished on the basis of texture, colour and degree of consolidation. In ascending order these comprise A, B, C and D (Figs. 4.3, 4.5).

4.4.1. Unit A

A homogenous, soft, pinkish-brown silty claystone with tuffaceous components. No internal structures were evident. Unit A was deposited from suspension in a low-energy paludrine,

lacustrine, or floodplain environment. It contains rare, poorly preserved bone fragments and stone artefacts. A sample from this mudstone, taken just beneath Unit B, yielded a fission track age of 0.88 ± 0.07 Myr BP (Morwood *et al*., 1998). This unit now provides the earliest dated evidence for hominins on Flores.

4.4.2. Unit B

Light-grey to white in colour, 1.6 - 2.2 m thick and fining-upward. Internally, Unit B consists of an amalgamated complex of sheets and lenses with variable grain-sizes and degrees of sorting. The basal part of the fossil-bearing Unit B consists of a 0.5-1.3 m thick layer of very poorly sorted, tuffaceous sandstone (Figs. 4.6 – 4.12). The erosional base consists of a weakly undulous, sharp erosional contact with the underlying silty claystone of Unit A. Eroded mudstone clasts derived from Unit A are abundantly present in the basal sandstone layers, and are at some places concentrated forming lenses with a clast-supported texture. The tuffaceous sand contains small pumice fragments, which in the northeast corner of Sector VIII are concentrated in a clast-supported pumice lens (Fig. 4.12). Besides mud clasts, the basal part of the sandstone contains

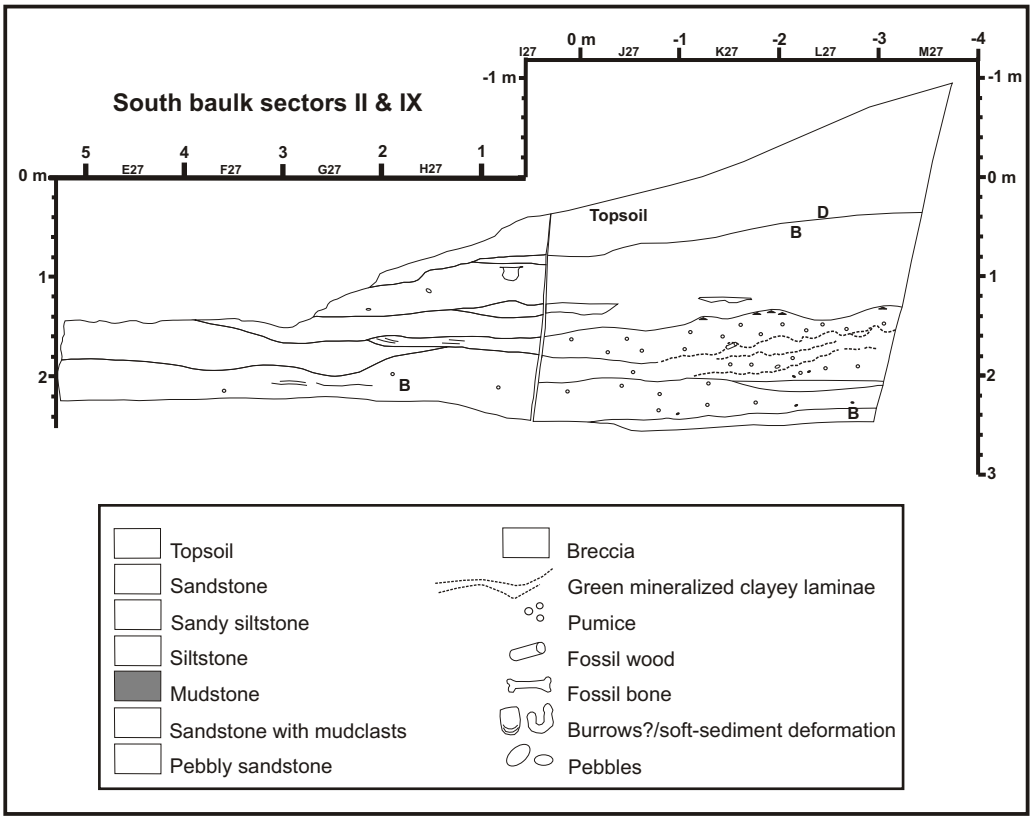

Fig. 4.6. South baulk of sectors II / IX and legend of the profiles shown in figures 4.6 - 4.12.

scattered sub-angular to sub-rounded volcanic clasts – natural andesite and basalt pebbles, and stone artefacts. A single rounded boulder with a maximum diameter of 20 cm at the basal contact (west wall of Sector II) suggests an (occasionally) highly energetic, depositional environment.

Sandy lenses and layers are generally 10 to 30 cm thick and are laterally traceable over one to ten meters. They can have concave or convex upper boundaries, and an undulous or irregular base (e.g. Figs. 4.10 - 4.12). Most sandstone lenses and layers are poorly sorted and do not exhibit internal sedimentary structures, though well-sorted, homogeneous and laminated sandy lenses do occur. In non-massive, sandy lenses, the observed sedimentary structures consist of parallel laminated streaks of medium-sorted sand or granules, low-angle cross-bedding (Fig. 4.12) or tabular cross-

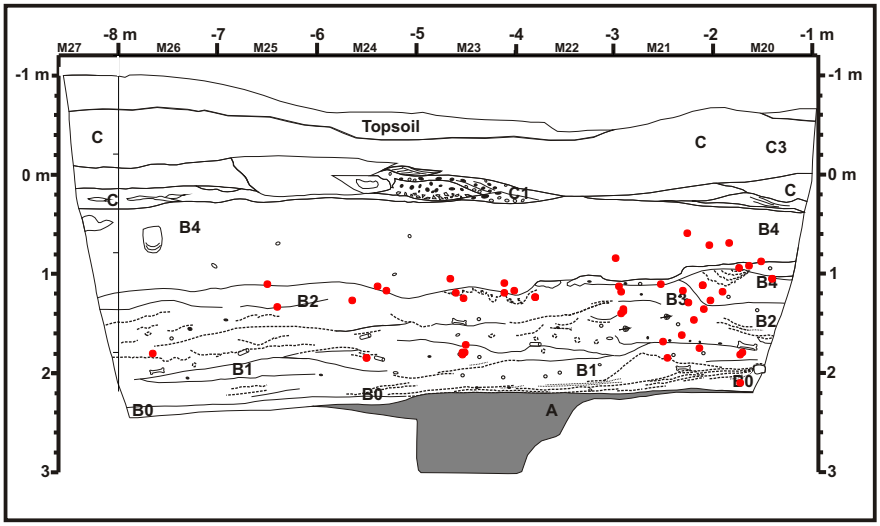

Fig. 4.7. West baulk of Sectors IX, VI and VII. For legend see Fig. 4.6 Red dots are projected fossil positions excavated from these three sectors

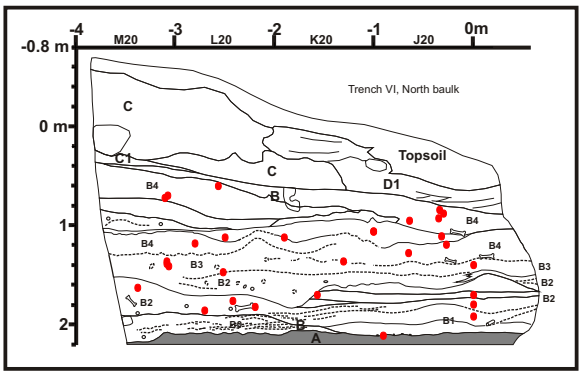

Fig. 4.8. North baulk of Sector VI. For legend see Fig. 4.6. Red dots are projected fossil positions excavated from sectors IV and VI between -1m > y >-4 m.

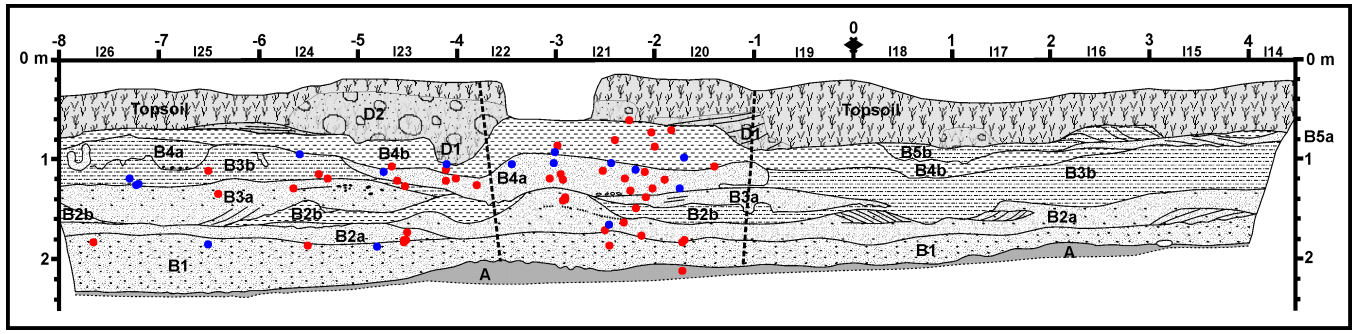

Fig. 4.9. West baulk of Sector II. For legend see Fig. 4.6. Red dots are projected fossil positions excavated from sectors VII, VI and IX (West of profile); blue dots represent fossils excavated from Sector II (East of profile). Note that in the right-hand side of the figure, the absence of red dots does not mean that no fossils were excavated here: this sector was excavated before 2004.

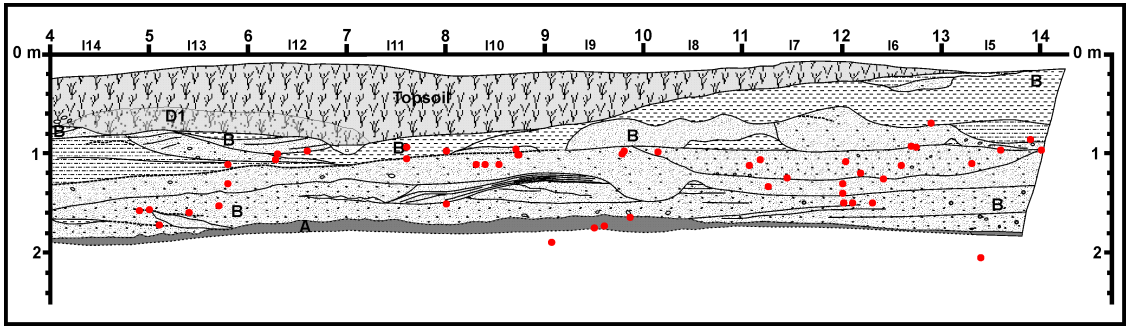

Fig. 4.10. West baulk of Sector III. For legend see Fig. 4.6. Red dots are projected fossil positions excavated from Sectors III and VIII.

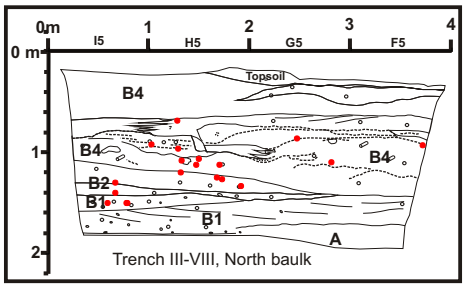

Fig. 4.11. North baulk of Sectors III / VIII. For legend see Fig. 4.6. Red dots are projected fossil positions excavated from Sectors III and VIII between 14m > y > 11 m.

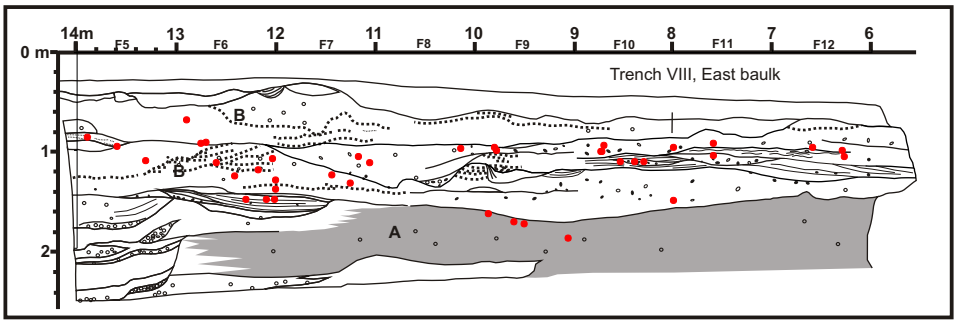

Fig. 4.12. East baulk of Sector VIII. For legend see Fig. 4.6. Red dots are projected fossil positions excavated from Sectors III and VIII.

bedding (Fig. 4.9, quadrants I15 - I18). In one profile the top of a sandstone lens, which is overlaid by sandy siltstone, has an undulous surface with internal wave-ripple structures (Fig. 4.6: quadrants K27-M27). Buried cliff-faces and over-steepened boundaries with a vertical relief of 10-30 cm also occur (e.g. Fig. 4.11, quadrant H5; Fig. 4.14), indicating considerable cohesiveness of sediments shortly after deposition.

In addition, Unit B contains many irregular, sometimes wavy crinkly, olive-green mineralized laminae up to 3 mm thick (Fig. 4.15A-E; in the profile drawings of Figs. 4.6 – 4.12 these are indicated by dashed lines). Some of the laminae are traceable over several meters (Fig. 4.13); some are stacked in repeating, irregular, concave or convex shaped structures (e.g. Fig. 4.7, quadrant M20 at 1 and 2 m below datum level); and some partly cover intracasts, bones and wood fragments (Fig. 4.7, 4.15A-B, E). They are interpreted as microbial mats (see below).

Stratigraphic differences between excavation profiles provide detailed information on the geomorphic history of the site. For instance, several sandy sub-units recognizable on the north-south profile laterally grade into siltstones and sandy siltstone to the west; while massive sandstone layers lacking internal structures in north-south profiles, split up in several westward off-lapping layers that are separated by microbial mat laminae, indicating breaks in deposition (Figs. 4.6, 4.8, 4.9). Furthermore, on the west side the lateral extension of individual recognizable sandstone lenses is generally limited, and the boundaries between lithological sub-units are more irregular. For instance, the basal sandstone layer of Unit B (designated "B1" in Figs. 4.8 – 4.9) can be traced for 22 m north-south (Figs. 4.9 – 4.10), but wedges out rapidly to the west (Fig. 4.8, bottom), as

does a 20 cm thick siltstone lens with microbial mat laminae that separates the pink tuffaceous mud of Unit A and sub-unit B1 (B0 in Fig. 4.8).

In addition, stratigraphic differences across the site provide palaeo-topography evidence. The basal layer of Unit B, for instance, is erosive and has cut down stepwise to the east: it is deepest in the northeast corner of Sector VIII (Fig. 4.12), where the deepest in-fill is of clast-supported lenses of intra-clasts and pumice fragments.

Towards the upper part of Unit B, sandy layers become better sorted, laterally less extensive and thinner, whereas well-sorted tuffaceous silt layers become the dominant facies. These silts are massive and do not show internal structures. The white siltstone layers and lenses tend to fill in existing relief, but may exhibit concave irregular eroded top surfaces as well. Occasionally, bone fragments and artefacts can be found embedded in these fine-grained silty layers and lenses, though there are relatively few fossils compared to the sandy layers (see Figs. 4.7 – 4.12).

In the upper siltstones, irregular-shaped, vertical sandy tubes with a maximum diameter of 7 cm (Figs. 4.6 – 4.8) represent soft-sediment intrusions (liquefied sediment injections triggered by earth-quakes), as described by Neuwerth *et al*. (2006). Soft-sediment deformation is also evident in the internal convolutions of laminated, sandy silts (Fig. 4.15F). In other sections, some sandy tubes may be rodent burrows.

The top of Unit B is eroded. It is overlain by massive siltstone with small lenses of breccia and sand (Unit C) or, where Unit C is not developed, by unconsolidated coarse pebbly sand and conglomerate of Unit D. Potholes eroded in the top of the white silts at the top of Unit B consist of cylindrical cavities with rounded pebbles at the base and topped up with loosely consolidated yellow coarse sand of Unit D: the sediments of Unit B were already strongly consolidated before erosion occurred.

4.4.3. Unit C

An erosional hiatus of unknown extent separates Units B and C. The latter has a complex internal structure with various lithological sub-units, including pink tuffaceous siltstone, lenses of breccia and sand, and unconsolidated sand (Figs. 4.7 and 4.8). Unit C cuts down at least 130 cm into the upper silts of Unit B, and the erosional boundary is sharp. It seems to represent an initial phase of fluvial scouring followed by rapid deposition of various volcanic products. Unit C has not yielded fossils or artefacts.

The most obvious difference between Unit B and C is the weaker consolidation of the latter, notably in the coarse clastics at its base, which comprise lenses of angular breccia and conglomerates of sedimentary intra-clasts. They are also different in colour: the sandstone and siltstones of Unit B are bright grey and white, respectively, whereas those of Unit C are pink, yellow, greenish or yellowish brown.

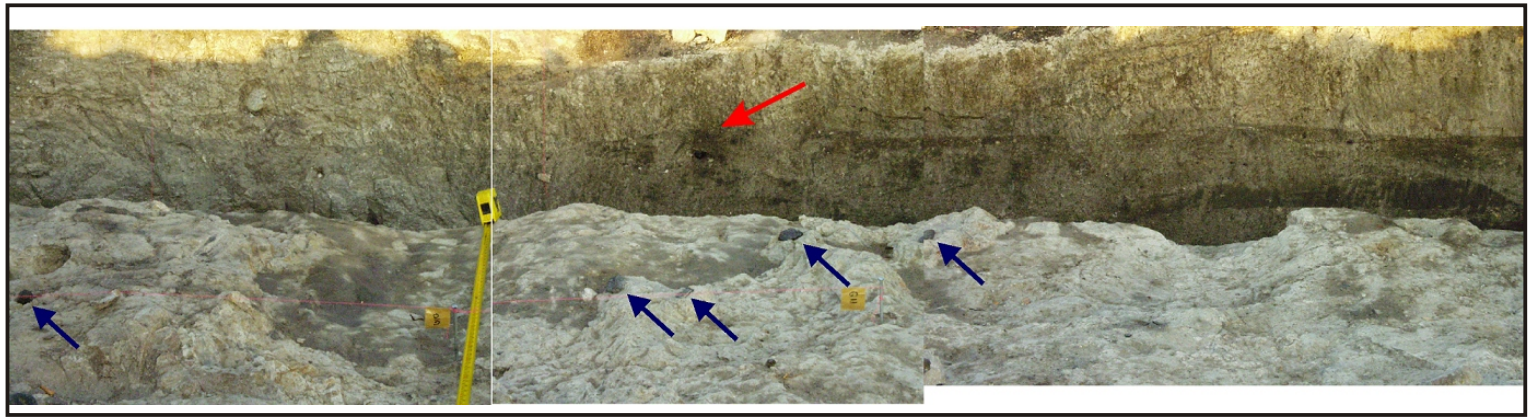

Fig. 4.13. Sector III/VIII: Undulous top surface of sandstone capped by green microbial mat lamina (dark surface) covered with white tuffaceous silt (light grey patches). The same lithological boundary is visible on the profile in the background (red arrow). Blue arrows point to stone artefacts embedded in the white tuffaceous silt.

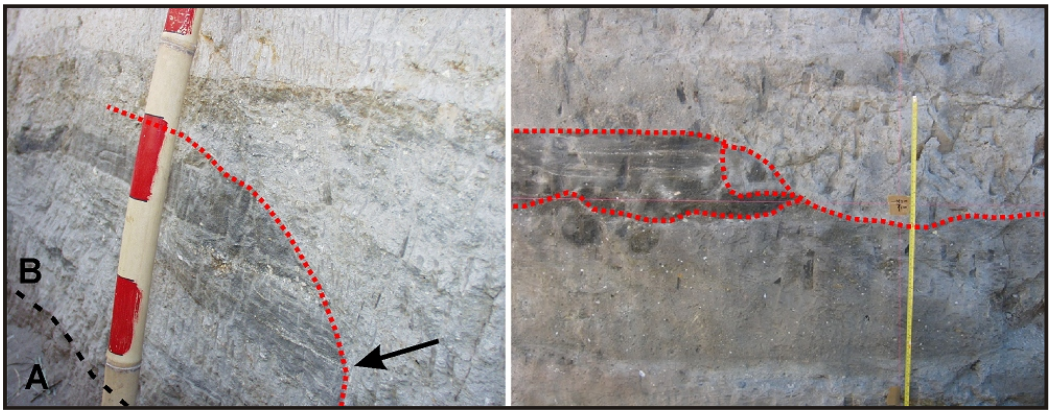

Fig. 4.14. Examples of steeply inclined cliff faces indicating considerable cohesiveness of the sediment during erosion. Left: Steeply inclined erosional contact (red dashed line, arrow) between two sandy sub-units of Unit B, as exposed in the west baulk of trench III (see also Fig. 4.10 quadrant I9). The top of the eroded sand lens consists of parallel laminated well-sorted sandstone, the overlying sand is poorly sorted. Right: Eroded dark grey laminated sand lens that is laterally bounded by homogeneous sand reworked from the lens, which is in turn covered by light grey tuffaceous silt. North baulk of sector VIII.

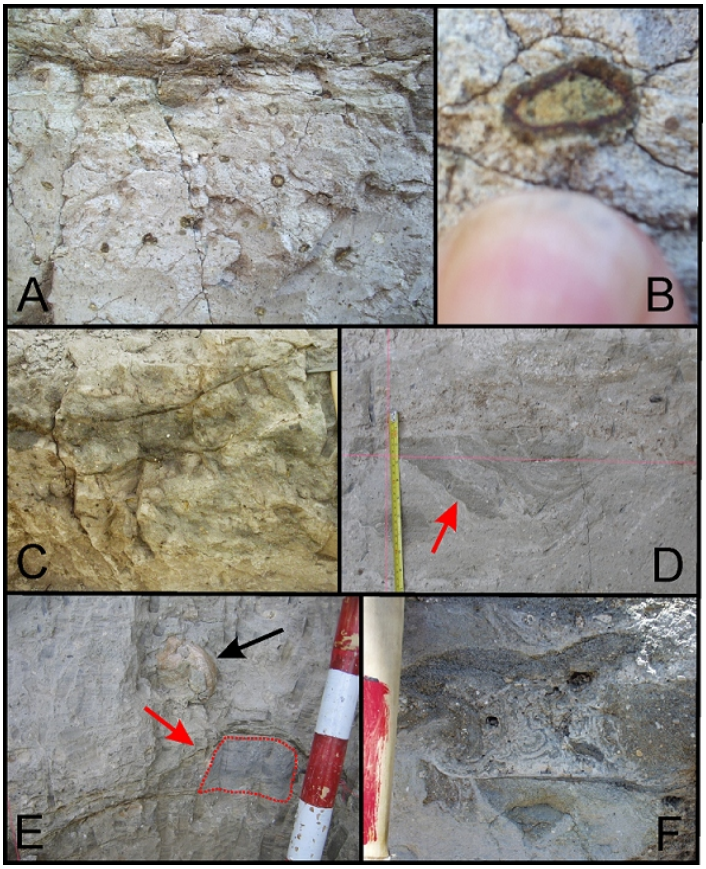

Fig. 4.15. Sedimentary structures related to microbial mats. A: Tuffaceous silt with sub-spherical coated intraclasts (onkolites). B: detail of onkolite. C: Irregular green laminae covering a sandy lens with a positive relief. D: Sandy silt alternating with concave wavy-crinkly laminae filling in a small channel (red arrow). E: Green laminae (red arrow) draped against an angular sandstone intraclast (red dashed line). Black arrow points to a Stegodon humerus head. F: Convolutions in coarse sandstone, possibly caused by soft-sediment deformation.

4.4.4. Unit D

Unit D comprises poorly consolidated, yellow-brown fluvial sand, pebbly sand and gravel that contain a few stone artefacts, but no fossils. It has a minimum thickness of 90 cm, but the top is overprinted by topsoil (Figs. 4.6 – 4.12). The pebbly sands show cross-bedding and the pebbles are sub-angular to sub-rounded with a maximum pebble diameter of 8 cm.

Unit D is clearly of fluvial origin and incised into the underlying Units C and B with a deeply and steeply incised, erosional contact. For instance, in the north baulk of Sector IV (Fig. 4.8), it cuts through the pink tuffaceous silt of Unit C into the upper part of Unit B, while further to the east Unit C has been entirely stripped. The erosional contact between Units B and D in the excavation and near Point S3 (Figures 4.2 and 4.3) is also characterized by potholes (Fig. 4.9, quadrants I22-I23; Fig. 4.16).

Fig. 4.16. Cross-cut of a pothole (red dashed line) eroded in consolidated white tuff of Unit B and filled with yellow-brown pebbly sand of Unit D (location S3 in Fig. 4.2). Note pebbles near the base of the pothole structure.

4.5. Lateral development of Units A, B, C and D

Units A and B extend for hundreds of meters, but the lithology and texture of the latter varies considerably. For instance, at the most southerly point where Unit B is exposed about 200 m southeast of the Mata Menge excavation (S5 in Figures 4.2 and 4.3), it is only 63 cm thick, and made up of two extensive sub-units that overlie a one meter thick interval of mudstones, corresponding to Unit A (Fig. 4.3). The lower sub-unit is a 35 cm thick, massive and well-consolidated layer of very poorly sorted, sandy mud with a non-erosive base, representing a mudflow. This is overlaid by a 30 cm thick, weakly laminated layer of white tuffaceous silt that is equivalent to the white tuffs in the upper part of Unit B in the excavation area. A weathered and poorly exposed sheet of conglomerates, with a maximum clast diameter of 7 cm, overlies the white tuffaceous silt. This conglomerate corresponds with Unit D, but the pebbly and coarse sands, characteristic of the unit in the excavation area, can only be identified in localized patches.

In another outcrop located 100 metres southwest of the excavation (S4 in Figures 4.2 and 4.3), a similar mudflow deposit, 20-30 cm thick with scattered boulders up to 15 cm in diameter and angular clasts overlies white tuffaceous silt, which is equivalent with the upper white tuffaceous silt of Unit B in the excavation area. The mudflow was partly eroded and undercut from the east, and then covered by several metres of pinkish tuffaceous mud (Fig. 4.17), the later being lateral equivalent with Unit C. In the same section, Unit D conglomerates cut down steeply into this pink mud for at least 4 m (Fig. 4.3). A similar down cutting feature can be observed in the north baulk of Sector VI in the excavation (Fig. 4.8).

About 140 m northeast of the excavation, there is another outcrop (S3 in Figures 4.2 and 4.3), where the pebbly sandstones of Unit D have infilled potholes eroded in a massive white tuffaceous silt that is the lateral equivalent of Unit B (Fig. 4.16). Here tabular cross-bedding is developed in the loosely

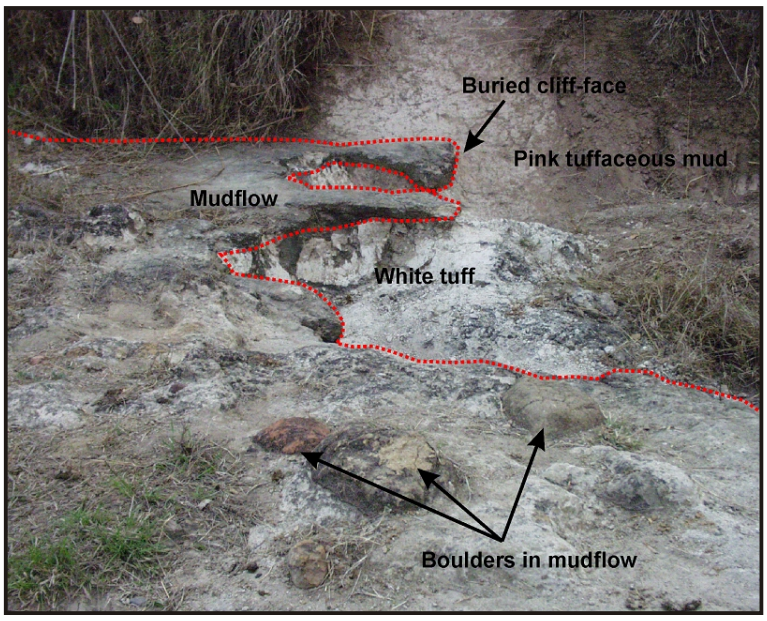

Fig. 4.17. Buried erosional cliff developed in mudflow deposit ca. 220 m southwest of Mata Menge in the same unit (Section S4 in Fig. 4.2). The white tuff underlying the mudflow constitutes the lateral equivalent of the fossil-and artefact-bearing layer at Mata Menge.

consolidated, pebbly sands, with foresets of up to 70 cm high (Fig. 4.18).

Near S3, four palaeo-current measurements could be taken on different foresets: 002º N, 030º NNE, 340º NNW and 354º N, all indicating a northward flowing river system, as does the eastward dipping erosive basal contact of Unit D, evident in the north baulk of Sector VI (Fig. 4.8). The steeply dipping basal contact of Unit D, the 70 cm high foresets and the potholes also indicate a confined river system with deeply incised, erosive channels and a coarse grained bedload.

4.6. Fossils

4.6.1. Stegodon and other vertebrate taxa

Between 1992 and 2006, a total of 169 *Stegodon* fossils were excavated at Mata Menge. Those excavated during the 2004-2006 field campaigns are listed in Tables 4.1 and 4.2, while the 1991-1994 finds are described in van den Bergh (1999).

Stegodon remains occurred throughout Unit B, including the well-sorted, tuffaceous silts, but were more common in the coarser-grained, basal sandstones (Figs. 4.7-4.12; while concentrations were found at the boundaries between sandy and tuffaceous silt layers. No articulated examples were found, many long bones were fragmented and, apart from isolated dental and tusk elements, only

Fig. 4.18. Tabular cross-bedding developed in the yellow-brown pebbly sandstones of Unit D, ca 140 m North of the Mata Menge excavation (location S3 in Fig. 4.2). Foresets are 70 cm high, indicating a comparatively large river system with a channel depth of at least several metres.

one skull fragment was recovered, a fragment of an occipital bone (MM04-32).

Other vertebrate remains recovered from Unit B include the mandibles, incisors and skeletal elements of the giant murid *Hooijeromys nusatenggara*, which total 15% of the Number of Individual Specimens (NISP). They are probably much more numerous than these figures indicate, but most were probably not recovered because excavated sediments were not sieved. Crocodile remains, specifically teeth and dermal scutes, comprise a further 5% of the NISP, and the excavations also yielded a single pelvis of an unknown bird species.

4.6.2. Non-vertebrate fossils

Poorly preserved fossil wood fragments are scattered throughout the sandstone layers and lenses of Unit B, but do not occur in the tuffaceous silts. The wood itself has decayed and is very poorly preserved. It is most evident as cylindrical molds up to 8 cm in diameter, with a partial filling of yellow substance, possibly vivianite (Fig. 4.5). In addition, poorly preserved imprints of leaves and grass, as well as the stalks and cone-like structures (strobili) of Equisetaceae (horse-tail; Isabel van Waveren, pers. comm.) are locally present: these plants usually prefer wet sandy soils, and some species are aquatic.

Phytoliths (opaline silica plant microfossils) are very well-preserved in four sediment samples analysed from Unit B (Fig. 4.19). Articulated epidermal silica skeletons are also common. This is indicative of low rates of weathering due to rapid burial following deposition and/or relatively little translocation (if any) from the original source of deposition. With the exception of MM-p-2, the phytolith assemblages are indicative of predominantly open woodland vegetation with an understorey of grasses, typical of present day monsoon environments (Table 4.3). Grasses are dominated by panicoid grasses in the Themeda/Imperata/Saccharum complex. The sandstone layer represented by MM-P-2 is characterised by a larger component of non-graminaceous vegetation, possibly due to wetter climatic conditions.

Unit B also contains freshwater gastropods, including *Brotia testudinaria* (von dem Busch, 1842; freshwater, running or agitated water), *Tarebia granifera* (Lamarck, 1822; freshwater, running to episodically stagnant) and an unidentified bassomatophoran landsnail (Frank Wesselink, Naturalis, pers. comm.).

4.6.3. Microbial mats

Green laminae are a conspicuous feature in Unit B sediments, both the sandstones and finer-grained clastics. Microscopic study of thin sections and SEM imaging of these laminae did not reveal remnants of diatoms or microbial filaments. However, on the basis of their morphology (e.g. wavy-crinkly and irregularly wrinkled surfaces) and evidence for cohesive behaviour, such as over-steepened surfaces (Schieber, 1999), these laminae are remnants of microbial mats.

Microbial mats are found in a range of environments (Schieber, 1999; Gerdes *et al*., 1994; Jones *et al*., 1997), such as marine intertidal flats, hypersaline coastal lagoons, alkaline lakes and hot springs, as well as more moderate conditions (Jorgensen et al., 1983; Neu, 1994). Micro-organisms

responsible for these mats, including light-dependent cyanobacteria, diatoms and various groups of sulphur bacteria, live in a biofilm of slime that is able to trap sediment particles. Microbial mats serve as stabilizing agents at the sediment-water interface: they prevent erosion under high energetic conditions, and maintain relatively steep underwater slopes of sediments that otherwise would slump (Figs. 4.14, 4.15).

4.7. Taphonomy of the *Stegodon* bone assemblage

4.7.1. MNI and bone representation

Horizontal tooth replacement in *Stegodon* (and elephants) means that the dental remains can be used to estimate the minimum number of individuals (MNI) and their age structure: the latter is based on the assignment of molars to one of 43 dental wear age stages (van den Bergh, 1999). Some *Stegodon* molars from Mata Menge can be attributed with confidence to the same individual because of morphological similarities and stratigraphic context. For instance, a left and right lower M3 (Nos. MM04-2 and 3) constitute a pair and were found close together with fragments of the mandibular rami (left ramus fragment No. MM04-31). Other molars of opposite and/or opposing jaw quadrants, were attributed to a single individual if they showed the same dental wear age stage, even if not recovered in close proximity or from the same stratigraphic sub-layer.

On the basis of excavated molars, at least 13 *Stegodon* individuals are represented in the faunal remains from all excavations at Mata Menge. However, no complete dentitions were found, and 80% of the number of molars (assuming that at any time at least 2 molars are in function in a single jaw quadrant), expected on the basis of the calculated MNI, were not recovered: if preserved they now lie outside the areas excavated. Similarly, for all other *Stegodon* skeletal elements, the number excavated can be expressed as a percentage of the number expected based on a MNI of 13. Table 4.4 provides the recovered/expected percentage for *Stegodon* skeletal elements at Mata Menge, as well as their Fluvial Transport Indices.

Fluvial Transport Indices (FTI) were devised by Frison and Todd (1986) for the skeletal elements of *Elephas maximus,* and are based on the distances moved by different skeletal elements in response to multiple fluvial current events. FTI values range from 0 to 100, and those elements with higher FTI values tend to be transported further than elements with lower values. Specifically, elephant skeletal elements with FTI values >75 are the sacrum, patella, astragalus, calcaneum, and cervical, thoracic and lumbar vertebrae, which are most prone to fluvial transport; elements with FTI values between 50 and 75 are the ribs, scapula, humerus, tibia and metacarpals; and elements with FTI values < 50 are the atlas, mandible, pelvis, radius, ulna and femur, which are the most resistant to movement. As might be expected, FTI groupings for elephants (used as a proxy for *Stegodon*) are very similar to the Voorhies Groups, established on the basis of transport experiments with bones of other ungulates (Behrensmeyer, 1990).

When the representation of skeletal elements at Mata Menge is graphed, and ranked according to their FTI values, it is clear that the large, compact and/or massive elements that are less prone to being transported by fluvial currents, such as pelvis, femur, mandibles and molars, are much better represented than the lighter, easily transportable elements, such as phalanges, tarsals, carpals, and

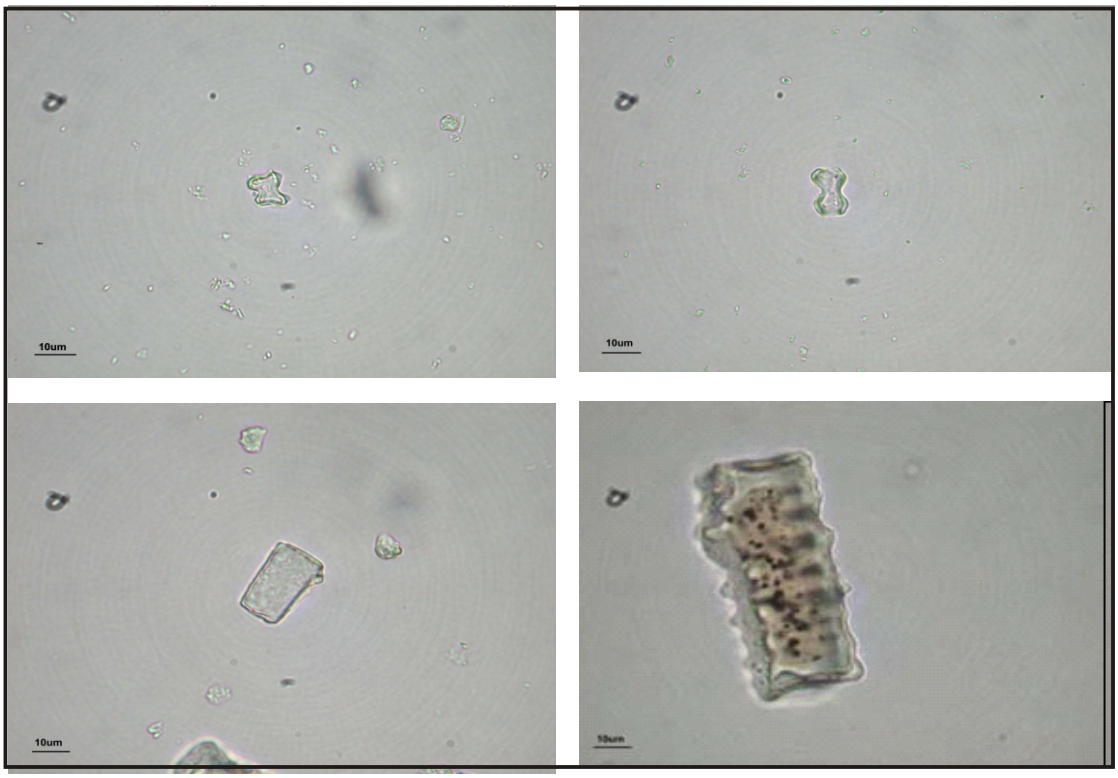

Fig. 4.19. Well preserved grass phytoliths from Unit B Trench IV. The upper right and left are bilobate morphotypes typical of panicoid grasses.

vertebrae (Figure 4.20). In fact, there is an inverse correlation between representation of elements at Mata Menge and their FTI (Fig. 4.21), showing that the easily transportable bones have been selectively removed from the site by water flow.

In order to investigate if the bone removal was distinct in the various depth intervals of the excavated fossil-bearing layer of Unit B, the number of bones of the three fluvial transport groups were plotted against stratigraphic depth (Fig. 4.22). Bones of all three groups are most numerous in the upper, fine-grained tuffaceous layers, while in the basal, poorly sorted and coarse sandstone interval, Group 3 bones that are least susceptible to fluvial transport, are much better represented than Group 1 bones, which are practically absent. This evidence indicates that easily transportable bones were preferentially winnowed from the intermittently high-energy, sheet flow deposits developed at the base of Unit B.

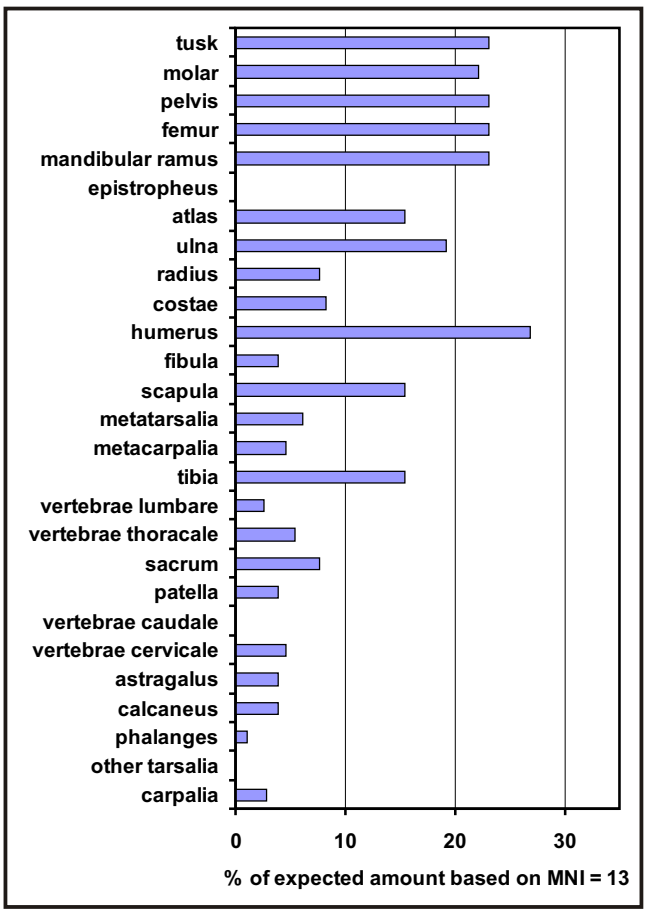

Fig. 4.20. Bone representation of postcranial elements excavated at Mata Menge, based on a MNI of 13 individuals. The various elements are ranked according to the Fluvial Transport Indices (FTI) of Frison and Todd (1986), with high FTI values (= likely to be transported) at the base to decreasingly lower FTI values towards the top

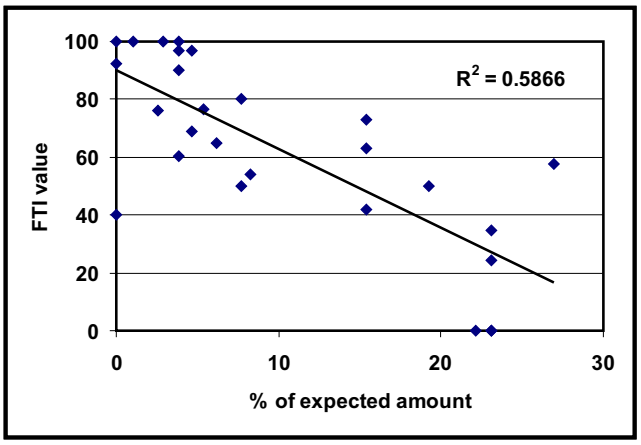

Fig. 4.21. Bone representation of skeletal elements excavated at Mata Menge (based on a MNI of 13 individuals) plotted against their FTI values. There is a significant correlation between the two parameters, showing that elements that are increasingly prone to fluvial transport are under-represented in the assemblage and have been selectively removed by water flow.

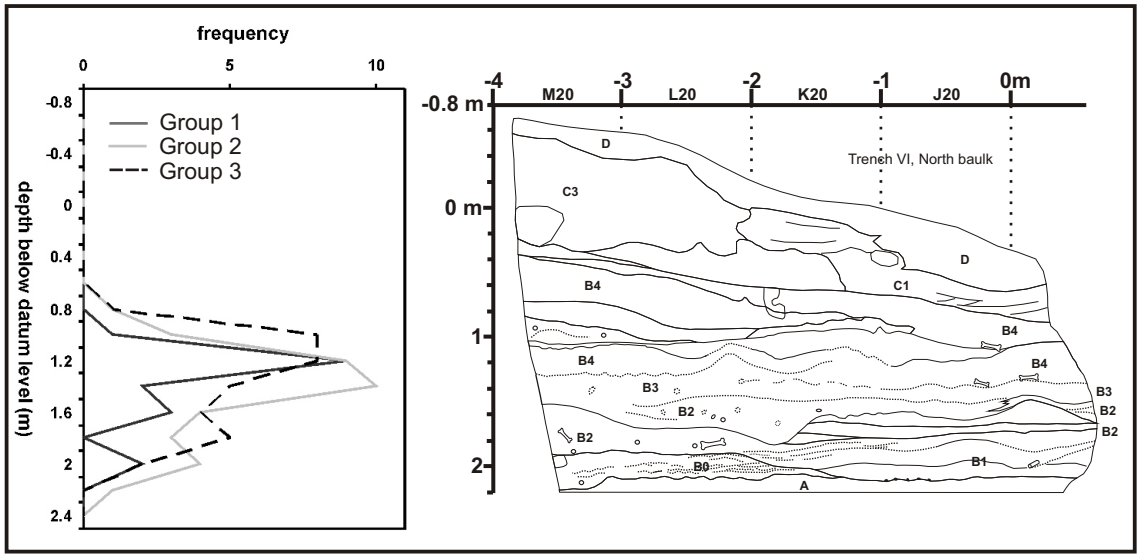

Fig. 4.22. Frequencies of skeletal elements of the three hydrodynamic bone classes distinguished per depth interval below datum level, and compared to the general stratigraphy to the right.

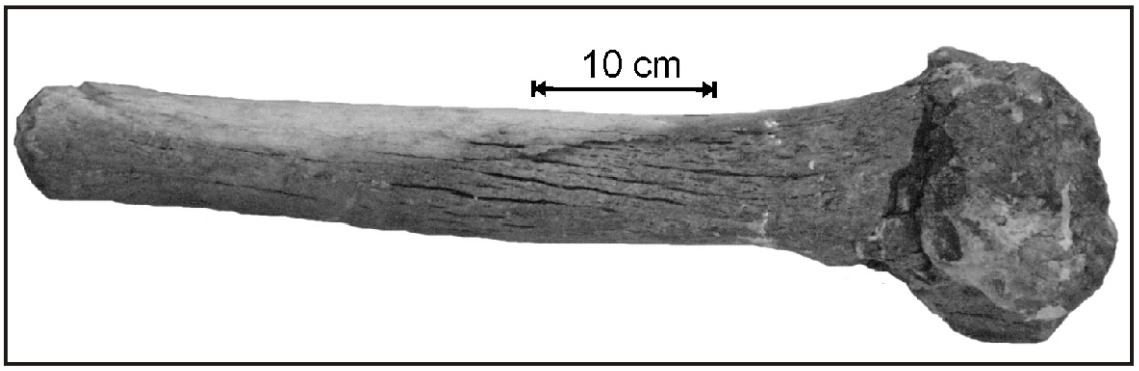

Fig. 4.23. Stegodon femur shaft with distal epiphyses still partly covered by sandstone and proximal epiphysis broken. Note the elongate desiccation cracks on the shaft and the ragged, abraded proximal fracture.

4.7.2. Bone breakage

Fossilization of faunal remains at Mata Menge is generally good, as is their surficial detail, but they are brittle and in a few instances there is evidence of secondary dissolution, for instance by recent root activity. When fossils were found in hard, strongly cemented sandstone, however, surficial damage during excavation was often unavoidable. Broken parts were immediately glued together, but often cortical bone was chipped off or pulverized, making it difficult to identify pre-burial abrasion or cut-marks. In contrast, bones found embedded in tuffaceous silt were more easily excavated without further damage.

Most bones have old pre-burial breaks. In fact 72 % of the NISP are incomplete or broken, as are

68% of the 38 excavated long limb bones (scapula, humerus, radius, ulna, pelvis, femur, tibia and fibula). Such breaks are often along irregular fractures that show signs of subsequent cracking and weathering, but usually not fluvial abrasion (Figs. 4.23). For instance, a mandible was found as two pieces in close proximity; though the pieces fit together, chips and flakes of bone along the edges of the fracture are missing (Figure 4.24).

Many specimens also had longitudinal cracks that indicate cortical bone desiccation prior to burial (Fig. 4.23); some from the basal sandstones of Unit B had evidence of fluvial abrasion; and some had microbial mat overgrowths showing that they were under water for some time. Bone modification by crocodilians bear certain characteristics, such as bisected toothmarks and

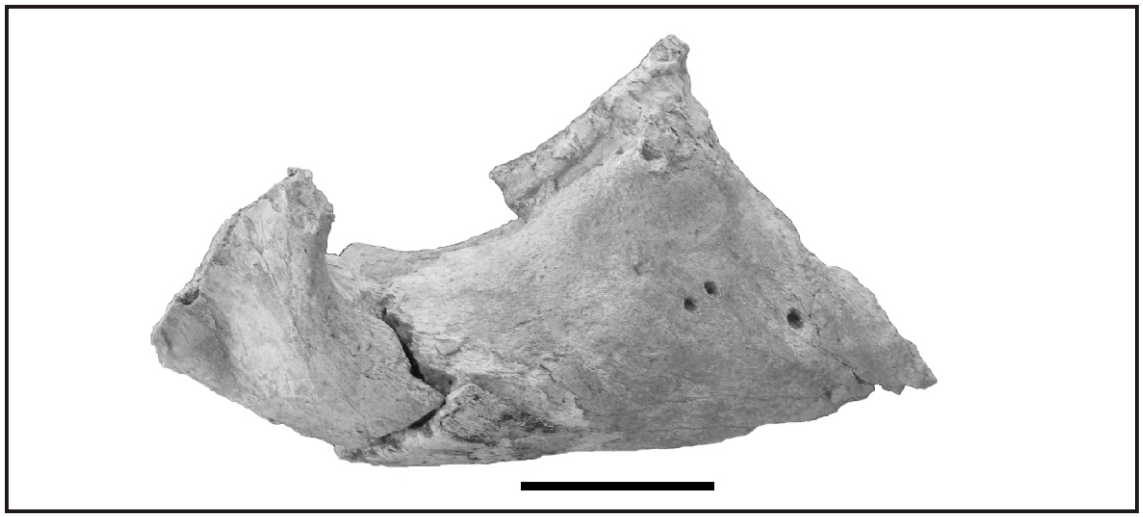

Fig. 4.24. Buccal view of a Stegodon right mandibular ramus of which a portion of the ascending ramus was found detached and close to the horizontal ramus. Edges of the fracture zone are eroded and flaked and the fit between the two fragments is incomplete. Scale bar is 10 cm.

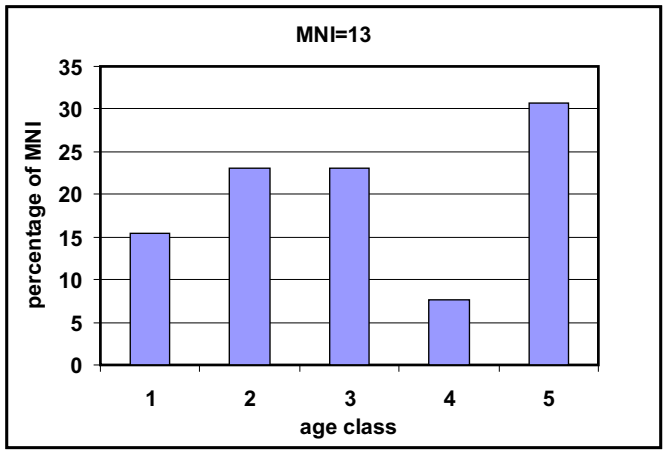

Fig. 4.25. Age structure of the Stegodon death assemblage of the Mata Menge excavation, based on a MNI of 13. Group 1 = juveniles; group 2 = young adults; group 3 = prime adults; group 4 = senior adults; group 5 = senile.

triangular projection of tooth punctures (Njau, 2006), none of which were observed on the Mata Menge bones.

None had cut-marks or fractures with clear impact points, incipient ring cracks or crushing that result from direct percussion with stones (Blumeschine & Selvaggio, 1988; Lyman, 1994). It seems that bones at Mata Menge were subject to pre-burial damage by exposure, trampling (presumably by *Stegodon*), fluvial transport and seasonally fluctuating lake levels.

4.7.3. Age structure of the Stegodon death assemblage

Dental wear stages in fossil *Stegodon* molars can be grouped into five age groups, each spanning approximately equal lengths of time (see van den Bergh 1999 for a detailed description). All 5 age groups occur in the Mata Menge assemblage, but very old individuals are over-represented and there are relatively few juveniles (Fig. 4.25). A similar age structure is evident in a time-averaged sample of 19 *Stegodon* individuals from other localities in the Soa Basin (van den Bergh, 1999).

Haynes (1987, 1991) work on death assemblages of both modern and fossil elephantoids is relevant here. He identified three types of patterned age profiles, designated as A, B and C. His Type A age profiles are characterized by a predominance (30%-60%) of juveniles and decreasing proportions of successively older age classes. This reflects the age profile of living populations. Such an age profile is evident for *S. sondaari* at Tangi Talo, where a volcanic eruption appears to have wiped out an entire population (van den Bergh, 1999; van den Bergh *et al*., 2001; chapter 3, this volume). In Type B age profiles the juvenile group greatly outnumbers mature animals, and may constitute more than 80% of the MNI. In such cases, the causes of death selectively affected juveniles. Such an age profile occurs at Liang Bua in West Flores, where over 90% of the *Stegodon florensis insularis* individuals are juveniles, which were brought into the cave and butchered by *Homo floresiensis* (van den Bergh *et al*., 2008). In contrast, Type C age profiles are characterized by the predominance of prime-age adults, while juveniles are rare. Such assemblages result from selective mortality over an extended period of time, or from non-selective mortality affecting a declining population with low numbers of juveniles.

The age structure of *Stegodon* at Mata Menge is not compatible with mass death resulting from a catastrophic event interpretation (Type A), or the selective mortality associated with predation by mammalian carnivores (Type B). If the absence of juvenile carcasses at Mata Menge is not due to their selective removal by Komodo dragons, crocodiles or hominins, then over-representation of old individuals at the site indicates optimal living conditions with low mortality rates for young individuals, and/or low regeneration rates.

4.8. Discussion and environmental interpretation

The sequential and lateral facies development, sedimentary structures, fossil content and taphonomic observations, all provide evidence for the palaeo-environment setting and geomorphic history of Mata Menge (Fig. 4.26).

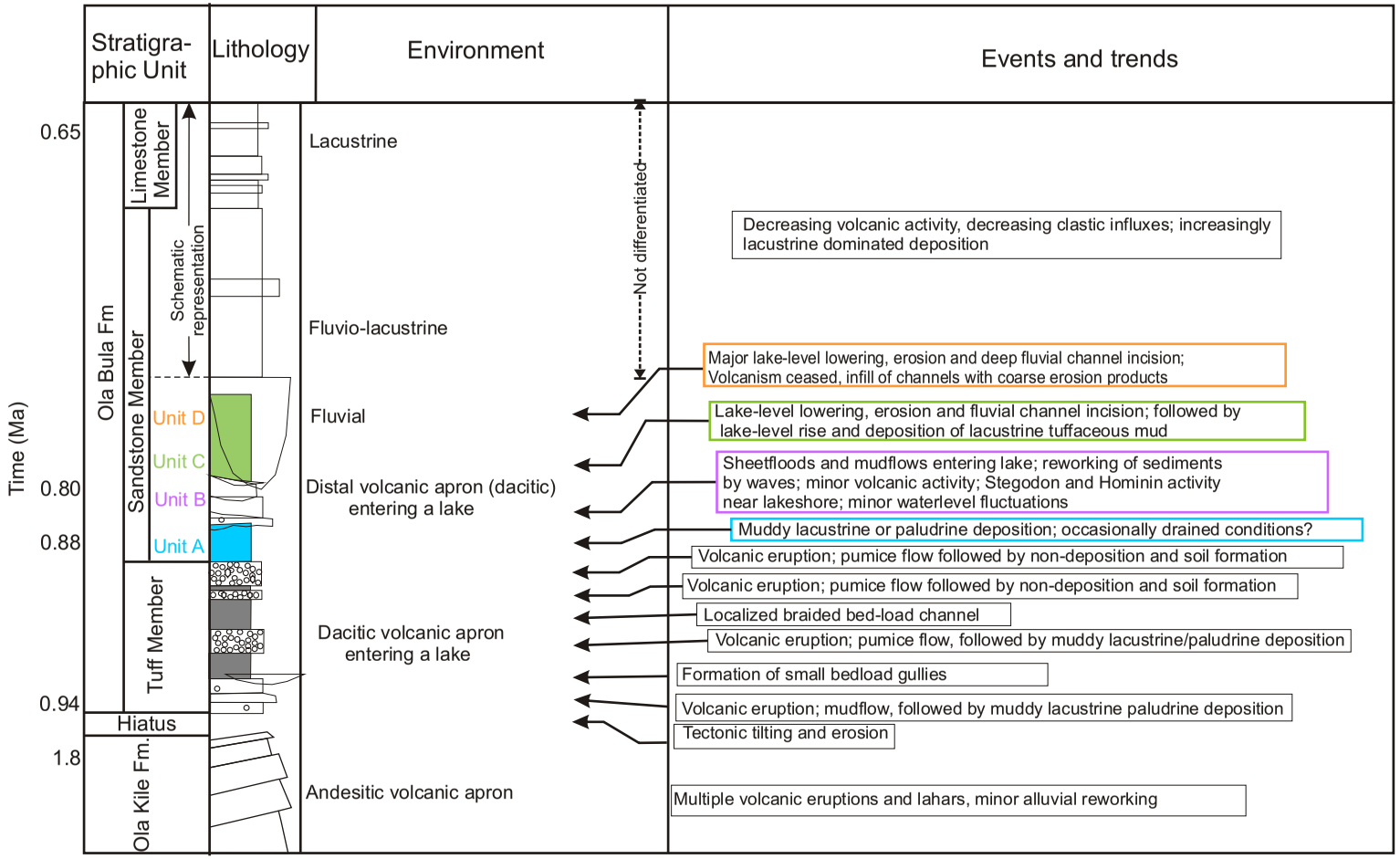

Fig. 4.26. General environmental interpretation and main environmental events and depositional trends in the surroundings of Mata Menge during deposition of the Ola Bula Fm, as derived from the lithological succession and sedimentological observations. Note that the top interval has not been studied in detail.

4.8.1. Environmental reconstruction before deposition of Unit B.

The facies geometry of the lower tuffaceous member of the Ola Bula Formation around Mata Menge is characterised by extensive syn-eruption sheets of tephra-rich, sandy flood-flow and debris-flow facies (Smith, 1987, 1991), alternating with fine-grained lacustrine tuffaceous muds and a few channelized gravel-bedload facies, the latter deposited during inter-eruption phases. While some of the massive pumice beds may have been deposited in hyperconcentrated flood-flows, the basal bed has characteristics of a pyroclastic flow (ignimbrite). Between eruption phases only limited incision and deposition in deeper bed-load channels is evident, and the fine-grained muds between successive pumice layers were deposited out of suspension in a lacustrine or paludrine environment. Depositional hiatuses are clearly marked by the well developed, red palaeosols overprinted on the upper two pumice beds, particularly in the marginal part of the Soa Basin west of Mata Menge.

4.8.2. Environmental reconstruction during deposition of Unit B

The unit sequence begins with a distal volcanic apron environment, in which readily available loose volcaniclastic materials were transported to the lake margin by shallow ephemeral streams, hyperconcentrated sheetflows and mudflows. At Mata Menge, these materials entered the lake from the northwest. The artefact-and *Stegodon*-bearing layer (Unit B) was deposited in a transitional fluvial to lacustrine environment - close to where a stream entered the lake. The energetic conditions (current and wave action) and sediment influxes were variable, depending on seasonal variations in fluvial discharge, fluctuating lake levels and changes in availability of loose volcanic tephra.

Deposition of the poorly sorted, basal tuffaceous sandstone sheets of Unit B occurred in poorly channelized hyper-concentrated sheet-flows. Occasionally, non-channelized mudflows also entered the lake, and are suggestive of a distal volcanic fan. The facies association of Unit B is interpreted as debris flows and hyper-concentrated flows (see Kataoka and Nakajo, 2002), with the basal sand sheets and lenses representing several phases of flow activity. During waning stages, shallow gullies developed on top of these rapidly deposited sheets, in which sediment concentrations decreased gradually, and better sorted low-angle and parallel laminated sands were deposited. During stages of decreased fluvial activity, the lakeshore deposits could be remodelled by waves eroding sandstones and undercutting small erosional cliffs. Under the influence of wave action the sandy shore sediments were locally re-shaped into coast-parallel beach ridges, which are oriented approximately north-south at the excavation site.

The internal microbial mat laminae indicate dominantly sub-aqueous conditions in a lake margin environment. Microbial activity likely contributed to early diagenetic processes increasing the cohesiveness of the subaqueous sediments, as seen in the occasional steep sediment boundaries and buried cliff faces in Unit B. Fossil gastropods indicate well-oxygenated, agitated water conditions along the lake margin.

Initially, available sediments mainly consisted of tuffaceous material, including large amounts of fine-grained tephra and pumice clasts. They likely represent reworked volcanic deposits first

deposited as air-fall tephra closer to the volcanic source. Currents were occasionally strong enough to transport coarser material, such as boulders up to 20 cm in diameter.

Higher in Unit B, well-sorted tuffaceous silts become the dominant facies, suggesting either a transgressive deepening of the lake and/or enhanced supply of fine-grained volcanic tephra. The low frequency of fossils in these tuffs, except near lower boundaries with sandstones, suggests rapid deposition and coverage of the bones. The existing relief of the lake margin, shaped by partial erosion of the stabilized microbial mat surfaces, beach ridges, erosional cliffs and shallow channels, was filled with silty material from suspension.

The few pebbles/angular clasts in the massive silt layers at the top of Unit B could have been transported by sheetfloods or mudflows entering the lake, then left as a lag when wave erosion eroded the surrounding matrix and rising lake levels led to their being covered with fine-grained sediment deposited from suspension. Alternatively, these clasts, many of which are artefacts, could have been brought to the lakeshore by hominins.

4.8.3. Events after deposition of Unit B

Following the deposition of the white tuffaceous silt at the top of Unit B, the lake-level dropped, resulting in fluvial down-cutting and erosion, as shown by the erosional surface separating Units B and C, and the unconsolidated, coarse clastic lenses at the base of Unit C. The lake level then seems to have risen again, and the eroded channel depressions were filled with fine-grained tuffaceous material.

A second cycle of down cutting and infill is represented by Unit D. The drainage of the lake seems to have been more pronounced and down cutting proceeded at least 4 m vertically down into older sediments. North of the excavation area, Unit C was completely eroded, while the top of the more resistant Unit B was also affected by erosion (potholes). The resulting valley incision was subsequently filled with the coarse clastics of Unit D, presumably because of decreased energetic conditions as the lake level rose again. By this time volcanic activity was more restricted or had ceased altogether, as the valley fill of Unit D consists of heavily weathered volcaniclastic products, with some non-volcanic components. Palaeo-current measurements indicate that the rivers, which deposited Unit D sediments at Mata Menge, flowed from south to north.

The shift from almost exclusively syn-eruption facies of the lower tuffaceous member to fluvio-lacustrine deposits of the middle member to the dominantly lacustrine conditions of the limestone member, suggests a gradual decrease in volcanic activity in combination with perhaps wetter conditions. However, periodic closure of the basin outlet by volcanic and or tectonic processes, variable subsidence rates or tectonic uplift of the northern hills and decreasing volcanism, all may have played a role in the fluctuating levels of the lake.

4.8.4. Hominins at Mata Menge

The sheer number of stone artefacts at Mata Menge and the fact that 58% were 'fresh' and only 12% heavily abraded shows that this former lakeside locale was a focus for hominin activities, including

import of materials for manufacture of stone tools (Moore and Brumm, 2007; Chapter 7 this volume). But there is no evidence that hominins played a role in the accumulation of *Stegodon* remains at the site or that associated stone artefacts were used to butcher animals. Instead, the faunal remains seem to have resulted from natural deaths of mainly old animals, and then been subject to weathering, trampling, moderate fluvial transport and winnowing; while retouch and usewear on some stone artefacts indicates that they were used in woodworking.

4.9. Conclusions

The sedimentological evidence presented above indicates that the stone artefacts and faunal remains excavated at Mata Menge accumulated along the western margin of a lake, which covered a large part of the Soa Basin; and at a time when explosive volcanic activity, as evident in the lower tuff member of the Ola Bula Fm, had largely ceased.

The lake itself was subject to minor fluctuations in water level, presumably due to seasonal changes in precipitation; and the majority of bones and artefacts excavated at Mata Menge are likely to have been deposited in the lake by streams and flash floods. In fact, just as the fossils and artefacts at nearby Boalesa were deposited at the junction of two water channels, so those at Mata Menge accumulated in close proximity to where a stream entered the lake (Morwood *et al.*, this volume). The lake was surrounded by open woodland vegetation with a predominance of grasses. Clearly, such a setting was also a favoured campsite for hominins. It was also a favoured watering location for animals, such as *Stegodon*, some of which died there. However, as yet there is no evidence that animals at the site were hunted or butchered by hominins.

Subaqueous bed-forms in the lake were stabilized by microbial mats, and wave-action along the margin caused minor erosion and the formation of beach ridges and erosional cliffs. At a later stage volcanic eruptions led to an abundance of available loose volcaniclastics that rapidly covered the exposed relief along the lake margin, and sealed in bones and artefacts.

Following deposition of the bone bed, the lake level dropped at least two times, perhaps signalling more arid periods or changes in the basin outlet. This led to erosion, followed by choking of the depositional system by a new influx of fine-grained volcaniclastics. Then nearby volcanism must have ceased altogether, and in combination with low lake levels, a period of deep incision by a south to north flowing confined river system followed. Faunal remains were not preserved in this setting dominated by erosion.

During later phases, lake-levels rose again, and around 680 kyr BP, a lake occupied the entire Soa Basin, as well as adjacent areas to the north. This coincided with minimal volcanic activity and initiated deposition of the limestone member that caps the Ola Bula Formation. The only known fossil vertebrate fossils associated with these limestones are of fish. Some time after 650 kyr BP, Lake Soa disappeared permanently when the present basin outlet was established, and the processes of river incision and erosion that characterise the area today began.

References

Argue, D., Donlon, D., Groves, C., Wright, R., 2006. *Homo floresiensis*: Microcephalic, pygmoid, *Australopithecus*, or *Homo*? *J. Hum. Evol.*, 51, 360–374.

Behrensmeyer, A.K. (1990). Transport-hydrodynamics: bones. In: D.E.G. Briggs and P.R. Crowther (Eds.) *Palaeobiology: a synthesis*: pp. 232-235. Oxford: Blackwell Scientific Publications.

Blumeschine, R.J. & Selvaggio, M.M. (1988). Percussion marks on bone surfaces as a new diagnostic of hominid behaviour. *Nature*, 333: 763-765.

Brown, P., T. Sutikna, M. J. Morwood, R. P. Soejono, Jatmiko, E. Wayhu Saptomo & Rokus Awe Due (2004). A new small-bodied hominin from the Late Pleistocene of Flores, Indonesia. *Nature*, 431: 1055-1061.

Brumm. A., F. Aziz, G. D. van den Bergh, M. W. Moore, M. J. Morwood, D. R. Hobbs, I. Kurniawan & R. Fullagar (2006). Lower Pleistocene stone artefacts from Mata Menge, Flores: implications for the behaviour of *Homo floresiensis. Nature,* 441, 624-628.

Falk, D., Hildebolt, C., Smith, K., Morwood, M.J., Sutikna, T., Brown, P., Jatmiko, Wayhu Saptomo, E., Brunsden, B. & Prior, F. (2005). The brain of *Homo floresiensis*. *Science* 308, 242–245.

Falk D, Hildebolt C, Smith K, Morwood M.J., Sutikna T, Jatmiko, Saptomo EW, Imhof H, Seidler H. & Prior, F. (2007). Brain shape in human microcephalics and *Homo floresiensis*. *PNAS*, 104: 2513-2518.

Frison, G.C. & L.C. Todd (1986). *The Colby mammoth site: taphonomy and archaeology of a Clovis kill in northern Wyoming.* Albuquerque: University of new Mexico Press.

Gerdes, G., W.E. Krumbein & H.-E. Reineck (1994). Microbial mats as architects of sedimentary surface structures. In: W.E. Krumbein, D.M. Paterson & L.J. Stal (eds.): *Biostabilization of sediments*. Druckerei Rösemeier, Bad Zwischenahn, Germany.

Haynes, G. (1987). Proboscidean die-offs and die-outs: age profiles in fossil collections. *Journal of Archaeological Science*, 14:659-668.

Haynes, G. (1991). *Mammoths, mastodons, and elephants: biology, behaviour, and the fossil record.* Cambridge, Cambridge University Press.

Hooijer, D.A. (1957). Three new giant prehistoric rats from Flores, Lesser Sunda Islands. *Zool. Meded.*, 35, 299-313

Hooijer, D.A. (1967). Indo-Australian insular elephants. *Genetica*, 38, 143-162.

Hooijer, D.A. (1972). *Stegodon trigonocephalus florensis* Hooijer and *Stegodon timorensis* Sartono from the Pleistocene of Flores and Timor. IandII. *Proc.Kon.Nederl.Akad.Wetensch.*, Ser.B, 75, 12-33.

Jones, B., M.R. Rosen & R.W. Renaut (1997). Silica-cemented beachrock from Lake Taupo, north island, New Zealand. *Journal of Sedimentary Research*, 67: 805–814.

Jørgensen, B.B., Reysbech, N.P. & Cohen, Y. (1983). Photosynthesis and structure of benthic microbial mats: microelectrode and SEM studies of four cyanobacterial communities. *Limnol. Oceanogr*., 28: 1075-1093.

Kataoka, K. & T. Nakajo (2002). Volcaniclastic resedimentation in distal fluvial basins induced by large-volume explosive volcanism: the Ebisutoge–Fukuda tephra, Plio-Pleistocene boundary, central Japan. *Sedimentology*, 49: 319–334.

Lyman, R.L. (1994). *Vertebrate taphonomy*. Cambridge University Press.

Maringer, J. & Th. Verhoeven (1970). Die Steinartefakte aus der *Stegodon*-Fossilschicht von Mengeruda auf Flores, Indonesien. *Anthropos*, 65: 229-247.

Moore, M.W. & A. Brumm (2007). Stone artifacts and hominins in island Southeast Asia: New insights from Flores, eastern Indonesia. *J. Hum. Evol*., 52: 85-102.

Morwood, M.J., Aziz, F., van den Bergh, G.D., Sondaar, P.Y. & J. de Vos (1997). Stone artefacts from the 1994 excavation at Mata Menge, West Central Flores, Indonesia. *Australian Archaeology,* 44: 26-34.

Morwood, M.J., O'Sullivan, P., Aziz, F. & Raza, A. (1998). Fission track age of stone tools and fossils on the east Indonesian island of Flores. *Nature*, 392: 173–176.

Morwood, M.J. & F. Aziz. (2001). *Archaeology and palaeontology of the Ola Bula region, Central Flores, Indonesia.* Final Report of the 1998-2001 joint research project, GRDC Bandung.

Morwood, M.J., R. P. Soejono, R. G. Roberts, T. Sutikna, C. S. M. Turney, K. E. Westaway, W. J. Rink, J.- x. Zhao, G. D. van den Bergh, Rokus Awe Due, D. R. Hobbs, M. W. Moore, M. I. Bird & L. K. Fifield (2004). Archaeology and age of a new hominin from Flores in eastern Indonesia. *Nature*, 431: 1087-1091.

Morwood, M.J., P. Brown, Jatmiko, T. Sutikna, E. Wahyu Saptomo, K. E. Westaway, Rokus Awe Due, R. G. Roberts, T. Maeda1, S. Wasisto & T. Djubiantono (2005). Further evidence for small-bodied hominins from the Late Pleistocene of Flores, Indonesia. *Nature*, 437: 1012-1017.

Muraoka, H., A. Nasution, M. Urai, M. Takahashi, I. Takashima, J. Simanjuntak, H. Sundhoro, D. Aswin, F. Nanlohy, K. Sitorus, H. Takahashi & T. Kosek (2002). Tectonic, volcanic and stratigraphic geology of the Bajawa geothermal field, central Flores, Indonesia. *Bull. Geol. Surv. Japan*, 53: 109-138.

Neu, T.R. (1994). Biofilms and microbial mats. In: W.E. Krumbein, D.M. Paterson & L.J. Stal (eds.): *Biostabilization of sediments*. Druckerei Rösemeier, Bad Zwischenahn, Germany.

Neuwerth, R., F. Suter, C.A. Guzman & G.E. Gorin, (2006). Soft-sediment deformation in a tectonically active area: The Plio-Pleistocene Zarzal Formation in the Cauca Valley (Western Colombia). *Sedimentary Geology*, 186: 67–88.

Njau, J.K. (2006). The relevance of crocodiles to Oldowan hominin paleoecology at Olduvai Gorge, Tanzania. PhD dissertation, Univ. of New Jersey.

O'Sullivan, P.B., M.J. Morwood, D. Hobbs, F. Aziz, Suminto, M. Situmorang, A. Raza & R. Maas (2001). Archaeological implications of the geology and chronology of the Soa basin, Flores, Indonesia. *Geology*, 29 (7): 607–610.

Schieber, J. (1999). Microbial mats in terrigenous clastics: the challenge of identification in the rock record. *Palaios*, 14: 3-12.

Smith, G.A. (1991). Facies sequences and geometries in continental volcaniclastic sediments. In: (R.V. Fisher & G.A. Smith, eds) *Sedimentation in Volcanic Settings*.

Smith, G.A. (1987). The influence of explosive volcanism on fluvial sedimentation: The Deschutes Formation (Neogene) in central Oregon. *Journal of Sedimentary Petrology*, 57: 613-629.

Sondaar, P.Y., G.D. van den Bergh, B. Mubroto, F. Aziz, J. de Vos & U.L. Batu, (1994). Middle Pleistocene faunal turnover and colonization of Flores (Indonesia) by *Homo erectus*. *Comptes rendues Ac. Sci. France*, série II, 319: 1255-1262.

Tocheri, M., C.M. Orr, S.G. Larson, T. Sutikna, Jatmiko, E.W. Saptomo, R.A. Due, T. Djubiantono, M.J. Morwood & W.L. Jungers (2007). The primitive wrist of *Homo floresiensis* and its implications for hominin evolution. *Science*, 317: 1743-1745.

van den Bergh, G.D., B. Mubroto, P.Y. Sondaar & J. de Vos (1996). Did *Homo erectus* reach the island of Flores? *Indo-pacific Prehist. Ass. Bull.*, 14: 27-36.

van den Bergh, G.D. (1999). The Late Neogene elephantoid-bearing faunas of Indonesia and their palaeozoogeographic implications. A study of the terrestrial faunal succession of Sulawesi, Flores, and Java, including evidence for early hominid dispersal east of Wallace's Line. *Scripta Geologica*, 117: 1-419.

van den Bergh, G.D., J. de Vos, F. Aziz & M.J. Morwood (2001). Elephantoidea in the Indonesian region: new *Stegodon* findings from Flores. In: *Proc. 1st Int. Congr. "The World of Elephants"*, Consiglio Nazionale delle Ricerche, Rome: 623-627.

van den Bergh, G.D., Rokus Due Awe, M.J. Morwood, T. Sutikna, Jatmiko & W. Saptomo (2008). The youngest *Stegodon* remains in South-East Asia from the late Pleistocene archaeological site Liang Bua, Flores, Indonesia. In: M.R. Palombo (ed.), Insularity and its Effects. *Quat. Intern.*, 182, 16-48.

Verhoeven, Th. (1968). Pleistozäne funde auf Flores, Timor and Sumba. In *Anthropica*, Gedenkschrift zum 100. Geburtstag von P.W. Schmidt, *Studia Instituti Anthropos*, 21: 393-403. St Augustin bei Bonn.

Table 4-1. *Stegodon florensis florensis molar elements excavated at Mata Menge between 2004-2006. x, y and depth coordinates are in meters and relative to the datum level. Positive x values are East of the datum level, positive y values are North of the datum; positive depth values are below the datum level. MGB = Geology Museum at Bandung; CTD = Culture and Tourism Department at Bajawa, Ngada District, Flores*

PSG Coll. No.	Storage	element	Sector	Quadrant	x (m)	y (m)	Depth (m)
MM04-1	MGB	molar: dex. M^3, post. Fragm.	III	I12	0.05	6.30	1.00
MM04-2	MGB	molar: sin. M_3, post. fragm.(pair with MM04-3)	II	J20	-0.35	-1.63	0.93
MM04-3	MGB	molar: mandible fragm with dex. M_3, anterior part shed (pair with MM04-2)	II	J20	-0.30	-1.51	0.88
MM04-4	MGB	molar: sin. M^3, post fragment (possibly pair with MM04-5)	I	?	?	?	?
MM04-5	MGB	molar: dex. M^3, intermed.fragm. Possibly pair with previous)	I	?	?	?	?
MM04-6	MGB	molar: Dex. M^1 posterior fragment	Outside excavation	-	-	-	-
MM04-8	MGB	Molar fragment	?	?	?	?	?
MM05-1	CTD	molar post dex M3 fragm.	VIII	F6	3.71	12.75	0.93
MM05-2	CTD	molar post dex M3 fragm.	VIII	F10	3.22	8.7	0.95
MM05-3	CTD	molar fragment	Outside excavation	-	-	-	-
MM05-43	CTD	molar: post M3 fragm.	VIII	H9	1.24	9.78	1
MM05-44	CTD	molar root fragm.	VIII	H5	1.28	13.6	0.96
MM05-45	CTD	molar ridge fragm.	VIII	?	?	?	?
MM05-52	MGB	molar: sin M1	VIII	H6	1.32	12.03	1.08
MM05-68	MGB	molar: M2 sin., posterior fragment	VI	J20	0	-1.7	1.8
MM05-72	MGB	molar: dex M2 in mandible fragm.	VI	L21	-2.42	-2.14	1.76
MM05-73	MGB	molar: dex M3 (same individual as MM05-(27)	VI	L20	-2.19	-1.72	1.83
MM06-2	MGB	molar fragment	VIII	G10	2.8	9.6	1.73
MM06-3	MGB	molar fragment	VIII	G9	2.9	9.5	1.75
MM06-4	MGB	molar fragment	VIII	G9	2.5	9.06	1.9
MM06-5	MGB	molar fragment	III	I9	0.9	9.86	1.65

Table 4-2. *Stegodon florensis florensis skeletal elements excavated at Mata Menge between 2004-2006. (MGB = Geology Museum at Bandung; CTD = Culture and Tourism Department at Bajawa, Ngada District, Flores)*

Coll No.	Repository	element	Sector	Quadrant	x	y	depth
MM04-7	MGB	Tusk, distal tip. 360 mm long fragm.	II	J20	-0.64	-1.73	0.95
MM04-9	MGB	Vertebra cervicale V	III	I13	0.87	5.40	1.60
MM04-10	MGB	Large proximal costa fragm. 610 mm long	I	?	?	?	?
MM04-11	MGB	Proximal costa fragm. 360 mm long	III	I7/I8	0.66	12.00	1.40
MM04-12	MGB	Scapula fragm.	?	?	?	?	?
MM04-13	MGB	Costa fragm. 250 mm long	?	?	?	?	?
MM04-14	MGB	Proximal costa fragm. 230 mm long	?	?	?	?	?
MM04-15	MGB	Large proximal costa fragm. 330 mm long	?	?	?	?	?
MM04-16	MGB	Distal costa fragm. 176x31x31 mm	?	?	?	?	?
MM04-17	MGB	Proximal costa fragm. (2 pieces). 305 mm long	?	?	?	?	?
MM04-18	MGB	Proximal costa fragm. 210x34x25 mm	?	?	?	?	?
MM04-19	MGB	Distal costa fragm. 176x36x13 mm	VI	I22/J22	0.00	-3.80	1.40
MM04-20	MGB	Dextral scapula fragm. 460+ mm long	I	?	?	?	?
MM04-21	MGB	Dextral fibula	II	H23	1.58	-4.80	1.87
MM04-22	MGB	Metatarsal IV, dextral	?	?	?	?	?
MM04-23	MGB	Proximal metatarsal II fragm.	III	I13/I14	0.70	5.00	1.57
MM04-24	MGB	Astragalus dextral	II	?	?	?	?
MM04-25	MGB	Uncinatum sinistral	III	I13	0.23	5.80	1.30
MM04-26	MGB	Trapezoideum sinistral	?	?	?	?	?
MM04-27	MGB	Dextral metacarpal III	?	?	?	?	?
MM04-28	MGB	Metacarpal fragment	?	?	?	?	?
MM04-29	MGB	Bone fragm. 75x60x24 mm	II	?	?	?	?
MM04-30	MGB	Proximal humerus fragm., dextral	III	I6/I7	0.66	12.00	1.30
MM04-31	MGB	Sinistral mandible ramus fragm. (same individ. as MM04-2 and MM04-3)	II	I20	0.44	-1.71	0.98
MM04-32	MGB	Skull fragm. (occipital) 107x86x25 mm	?	?	?	?	?
MM04-33	MGB	Vertebra thoracale	III	I14	0.91	4.90	1.58
MM04-34	MGB	Sinistral scapula	III	I13	0.54	5.70	1.53
MM04-35	MGB	Costa fragm. 125x24x12 mm	II	?	?	?	?
MM04-36	MGB	Proximal costa fragm. 145x22x11 mm	I	?	?	?	?
MM04-37	MGB	Distal costa fragm. 115x34x16 mm	?	?	?	?	?
MM04-38	MGB	Costa fragm. 106x34x14 mm	?	?	?	?	?
MM04-39	MGB	Distal costa fragm. 73x27x15 mm	?	?	?	?	?
MM04-40	MGB	Vertebra cervicale fragment	II	?	?	?	?
MM04-42	MGB	Sinistral femur (caput lacking)	IV	I22/J22	0.00	-3.80	1.70
MM04-43	MGB	pelvis fragm.: Sin. innominate	III	I6/I7	0.78	12.10	1.50
MM04-44	MGB	pelvis fragm.: Ilium fragm.	III	I6/I7	0.58	12.01	1.50
MM04-45	MGB	Sinistral tibia fragm., dist. epiphysis lacking	IV	I22/J22	0.00	-3.20	1.92

Table 4-2, continued

Coll No.	Repository	element	Sector	Quadrant	x	y	depth
MM04-46	MGB	Dextral femur diaphysis fragm.	III	I6/I7	0.77	12.30	1.50
MM04-47	MGB	Sacrum	II	?	?	?	?
MM04-48	MGB	Large sinistral costa fragm. 615 mm long	I	I30	0.35	-11.20	2.11
MM04-49	MGB	Dextral ulna	I	?	?	?	?
MM04-50	MGB	Humerus	I	?	?	?	?
MM05-4	CTD	dex mandible fragm. (juv.)	VIII	I/H6	1.02	12.7	0.92
MM05-5	CTD	vertebra thoracale (last one?)	VIII	H10	1.02	8.39	1.11
MM05-6	CTD	vertebra thoracale fragm.	VI?	L21	-2.8	-2.3	1.18
MM05-7	CTD	vertebra thoracale fragm.	VIII	H7	1.69	11.06	1.12
MM05-8	CTD	vertebra lumbale fragm.	IX	J22/23	-0.98	-4	1.18
MM05-9	CTD	proximal tusk fragm.	VIII	G5	2.71	14.01	0.96
MM05-10	CTD	tusk fragm.	-	?	?	?	?
MM05-11a	CTD	costa fragm., anterior region (3 or 4)	outside trench	A13	8.5	5.1	1.2
MM05-11b	CTD	costa fragm.	outside trench	A13	?	?	?
MM05-12	CTD	costa fragm. prox, sin.	VI	K21	-1.3	-2.09	1.37
MM05-13	CTD	costa fragm. prox, midthoracic	VIII	G5	2.8	13.31	1.1
MM05-14	CTD	costa fragm. prox, midthoracic	VIII	F10/11	3.66	8	0.97
MM05-15	CTD	costa fragm., midthoracic	VIII	H7	1.67	11.44	1.25
MM05-16	CTD	costa fragm., midthoracic	VI	M21	?	?	?
MM05-17	CTD	costa fragm., posterior thorax	VI	M21	?	?	?
MM05-18	CTD	costa fragm., midthoracic	VI	M21	-3.06	-2.92	1.41
MM05-19	CTD	costa, midthoracic	VI	M21	-3.08	-2.9	1.39
MM05-20	CTD	costa, (3 or 4)	VI	L21	-2.7	-2.46	1.86
MM05-21	CTD	costa fragm.	VIII	H13	1.1	5.8	1.11
MM05-22	CTD	costa fragm.	VIII	F10	3.71	8.53	1.11
MM05-23	CTD	costa fragm.	VI?	J21	-0.65	-2.02	1.28
MM05-24	CTD	dorsal spine vertebra fragm.	VIII	H6	1.31	12.18	1.2
MM05-25a	CTD	dorsal spine vertebra fragm.	IX	J22	-0.8	-3.79	1.25
MM05-25b	CTD	dorsal spine vertebra fragm.	IX	J22	-0.8	-3.79	1.25
MM05-26	CTD	mandible? Fragm.	VI	K21	-1.57	-2.5	1.7
MM05-27	CTD	ulna dex. fragm.	VIII	H8	1.94	10.14	0.98
MM05-28	CTD	sin humerus fragm. (caput)	VI	L21	-2.52	-2.19	1.48
MM05-29	CTD	vertebra arcus fragm.	VI?	K/J20	-1	-1.4	1.06
MM05-30	CTD	scapula sin, prox. fragm.	VIII	H13	1.8	5.1	1.72
MM05-31	CTD	ulna , dex.	VII	J25	-0.35	-6.4	1.34
MM05-32	CTD	humerus dex, distal fragm.	VIII	F11	3.04	7.6	1.05
MM05-33	CTD	femur sin, diaphysis fragm.	IX	J/I23	0	-4.1	1.1
MM05-34	CTD	femur fragm.: caput femoris	IX	J/I23	0	-4.1	1.2
MM05-35	CTD	femur shaft, fragm.	VIII	H7	1.91	11.25	1.33
MM05-36	CTD	dorsal spine vertebra thoracale fragm.	IX	K24	-1.23	-5.3	1.18
MM05-37	CTD	costa 1 fragment	VIII	H6	1.46	12.6	1.12
MM05-38	CTD	costa fragm., anterior region (3 or 4)	IX	L23	-2.79	-4.6	1.2
MM05-39	CTD	costa prox. fragm., midthoracic	IX	J23	-0.1	-4.53	1.8
MM05-40	CTD	humerus dex, diaphysis fragm.	IX	J/I23	0	-4.51	1.8
MM05-41	CTD	costa fragm.	VII	J/I26	0	-7.65	1.82
MM05-42	CTD	tibia sin	IX	J/I23	0	-4.53	1.83
MM05-46	CTD	mandible fragm. of horizontal ramus	VII	?	?	?	?

Table 4-2, continued

Coll No.	Repository	element	Sector	Quadrant	x	y	depth
MM05-47	CTD	tusk fragm.	VII	J25	-0.64	-6.5	1.11
MM05-48	MGB	tibia sin	VI	K/J20	-1	-1.4	1.06
MM05-49	MGB	ulna dex prox fragm., + shaft	VI?	L21	-2.5	-2.1	1.12
MM05-50	MGB	costa I, sin	VI	M21	-3.08	-2.9	1.37
MM05-51	MGB	tusk	IX	L23	-2.77	-4.52	1.26
MM05-53	MGB	atlas	IX	J23	-0.29	-4.16	-1.3
MM05-54	MGB	maxilla sin fragm.	IX	J23	-0.29	-4.16	-1.3
MM05-55	MGB	vertebra thoracale	VIII	H10/11	1.09	8	1.51
MM05-56	MGB	calcaneum dex	VIII	G12	2.33	6.6	0.97
MM05-57	MGB	Metacarpal IV dex.	VIII	H6	1.27	12.9	0.69
MM05-58	MGB	Metatarsal III sin.	Outside Excav.	-	-	-	-
MM05-59	MGB	second phalange II	VIII	H7	1.49	11.17	1.06
MM05-60	MGB	Metatarsal V sin	VIII	H9	1.8	9.8	0.97
MM05-61	MGB	Trapezoideum sin.	VIII	H12	1.3	6.28	1.06
MM05-62	MGB	distal humerus fragm. dex., lat. Condyle	VIII	G11	2.77	7.6	0.93
MM05-63	MGB	costa (posterior mid-thoracic)	VI	M21	?	?	1.4
MM05-64	MGB	costa fragment (posterior)	VI	M21	?	?	1.4
MM05-65	MGB	pelvis sin fragm. (ilium)	IX	K24	-1.98	-5.38	1.14
MM05-66	MGB	radius sin, proximal fragm.	VI	M21	-3.37	-2.31	1.63
MM05-67	MGB	Uncinatum (=hamatum =unciforme) dex.	VIII	M12	1.15	8.3	1.11
MM05-68	MGB	tusk fragm.	IX	?	?	?	?
MM05-69	MGB	tusk fragm.	VI	J20	-0.9	-1.72	2.11
MM05-70	MGB	vertebra cervicale	IX	K24	-1.39	-5.5	1.86
MM05-71	MGB	vertebra thoracale post. part(complete)	IX	K24	-1.39	-5.5	1.86
MM05-74	MGB	pelvis sin large fragm.	VIII	H6	1.72	12.41	1.26
MM05-75	MGB	radius sin	IX	J23	-0.2	-4.5	1.73
MM05-77	MGB	hyoid	VI	J20	?	?	?
MM05-99	MGB	small tusk fragment	VI	L20	?	?	?
MM06-1	MGB	phalanx	III	I5	0.3	13.4	2.05
MM06-6	MGB	phalange	VIII	?	?	?	?

Table 4.3. Summary of phytolith analysis of samples collected from Unit B, Trench IV Matamenge.

Sample	Layer description	Gramineae	Cyperaceae	Gramineae/Non-Gramineae	Non-Gramineae
MM-p-1	Upper white tuffaceous silt	25	3	19	53
MM-p-2	Sandstone	12	0	18	70
MM-p-4	Transitional between sandy layer and layer with microbial mats	27	2	24	47
MM-p-3	Basal poorly sorted pebbly sandstone	37	1	12	49

Table 4-4. Fluvial transport indices of Stegodon skeletal elements and their relative presence in the Mata Menge fossil assemblage based on a MNI of 13 individuals.

Bone	FTI	nr in 1 skeleton	expected amount	Presence %
carpalia	-	16	208	6
other tarsalia	-	10	130	0
phalange	-	22	286	3
calcaneus	100	2	26	1
astragalus	96.83	2	26	1
vertebra cervicale	96.64	5	65	3
vertebra caudale	92.43	22	286	0
patella	90.19	2	26	1
sacrum	80.11	1	13	1
vertebra thoracale	76.43	20	260	14
vertebra lumbare	76.21	3	39	1
tibia	72.84	2	26	4
metacarpalia	68.83	5	65	3
metatarsalia	-	5	65	4
scapula	62.95	2	26	4
fibula	60.19	2	26	1
humerus	57.77	2	26	7
costa	53.98	40	520	43
radius	49.95	2	26	2
ulna	49.95	2	26	5
atlas	41.97	1	13	2
epistropheus	-	1	13	0
mandible	34.56	2	26	6
femur	24.26	2	26	6
pelvis	0	2	26	6
molars	skull: low number	8	104	23
tusk	skull: low number	2	26	6